ACKNOWLEDGMENTS

We would like to begin by thanking our principal advisor, Professor Adrain S. Onas for his enthusiasm throughout this project. We would also like to thank Pete Melvin at Morrelli and Melvin Design and Engineering for providing the AC50 foil geometry used in this analysis. Thanks also to Tim Yen at CD Adapco who provided extremely valuable support and direction in the use of Star CCM+.

ABSTRACT

This thesis analyses the steady state fluid structure interactions, FSI, of high-performance sailing hydrofoils. This was performed by evaluating an isotropic, CV-style sailing hydrofoil, similar to those being used on the AC 50's, which will be competing in the 2017 Americas Cup. The FSI analysis was completed using the multi-physics simulation software, StarCCM+. The results from the FSI study are compared to a CFD analysis of the un-deformed foil, to determine the value of the FSI study. The deformed foil performance varied significantly enough at speeds of 30 knots and above to warrant a FSI study.

TABLE OF CONTENTS

LIST OF FIGURES

LIST OF TABLES

NOMENCLATURE

AC 72	America's Cup Class Yacht
CAE	Computer Aided Engineering
CFD	Computational Fluid Dynamics
FSI	Fluid Structure Interaction
FEA	Finite Element Analysis
FEM	Finite Element Method
FRP	Fiber Reinforced Polymer
HT	Hyper Threading
IMOCA	International Monohull Open Class Association
NACA	National Advisory Committee for Aeronautics
ORMA	Ocean Racing Multihull Association
RANS	Reynolds Average Naiver Stokes
c	Foil Chord length
i	Fluid Internal Energy
U_{FS}	Free Stream Velocity
T	Temperature
∇	Dell Operator
V_∞	Free Stream Velocity
u	Longitudinal Component of Velocity
v	Transverse Component of Velocity
w	Vertical Component of Velocity, Downwash Velocity
k	Thermal Conductivity
g	Acceleration Due to Gravity
P	Fluid Absolute Pressure
Star-CCM+	Viscous CFD Program
C_d	Drag Coefficient
C_l	Lift Coefficient
L'	Lift per Unit Span

D’	Drag per Unit Span
Γ	Circulation
μ	Fluid Dynamic Viscosity
nν	Fluid Kinematic Viscosity
ρ	Fluid Density
σ_{ij}	Normal Stress on Ith Face in Jth Direction
τ_{ij}	Shear Stress on Ith Face in Jth Direction
ϕ	Viscous Dissipation

INTRODUCTION

The realm of high-performance sailboat design is relatively small in the world of naval architecture for two main reasons, its complexity in balancing the forces between two fluids in order to maximize performance and the small scale of the market. However, these two attributes are almost exclusively what drives racing yacht designers to pursue the dream of creating the world's fastest naturally-powered water craft.

The lack in market scale and a low budget ceiling often force designers to make compromises in their design process. The challenging aspect of limited funding is deciding what areas of the design can be simplified, while still maintaining a safe and high-quality product. This thesis project examines the value of Fluid Structure Interaction (FSI) analysis, with a focus on sailing hydrofoils. FSI is a computationally expensive, iterative process that, in this case, analyzes the forces imparted on a foil by a moving flow field, then examines the deflection of the foil from the calculated pressure and shear forces; it repeats these processes until the deflection and forces converge to a steady-state equilibrium.

Hydrofoils provide vertical lift to raise racing sailboat hulls clear of the water, greatly reducing drag. Since hydrofoils support the entire weight of the boat, along with the forces induced by the sails, they are a prime candidate for consideration in the process of FSI analysis. The CV hydrofoil is recognized as the standard for today's leading edge racing catamaran designs. In addition, when discussing this topic with industry professionals, it became apparent that leading designers are considering a variety of implementations of FSI, especially at the highest level of sailing design, the America's Cup.

OBJECTIVES

The objective of this thesis is to couple a CFD analysis with a FE analysis, to complete a FSI study of a CV hydrofoil. A secondary goal of this thesis is to evaluate the necessity of considering FSI, through comparison between an undeformed CFD analysis and a deformed FSI analysis. This thesis builds on past Webb Institute CFD theses on foils, implementing the same style of foil with the addition of FEA of the structure to examine the effects of deformation on hydrodynamic performance.

BACKGROUND

VERTICAL-LIFT-PRODUCING DAGGERBOARDS

A recent development in yacht design is the addition of a horizontal wing element on daggerboards to help produce vertical lift, while simultaneously providing the required side force. The advantage of this type of arrangement is the effective reduction in displacement, and subsequent reduction of resistance, because of the vertical lift produced by the daggerboard. This horizontal wing element can also significantly increase heave stability, even when a minimal amount of vertical lift is being generated.

Lifting foils were first implemented on sailing craft in the mid-1950s by the U.S. Navy. It wasn’t until the 1980s that hydrofoils were first seen on sailing craft, after designers began experimenting with simple, constant-curvature lifting foils on catamarans. Late in the 1990s, the Ocean Racing Multihull Association (ORMA) 60 trimaran class provided the first real demonstration of the benefits of lifting foils (Figure 1). Although the foils used in this class produced small amounts of vertical lift, as compared to the vessels’ displacement, they showed obvious performance benefits.

Foiling

If enough vertical lift is produced, the hull can be fully lifted out of the water, effectively replacing displacement hull resistance with much less significant slender body foil resistance. This mode of operation is called foiling, and a vessel that is supported only through vertical lift produced by hydrofoils is considered to be fully foiling. The vertical lift generated replaces the buoyancy force of the displaced volume, reducing the waterplane area and thus the effects waves have on the hull, resulting in a vessel with exceptional heave stability.

Figure 1. ORMA 60 with lifting foils
Source: Charterworld.com

Lifting Foil Profiles

Lifting foils have developed increasingly complex shapes since their first generation, as constant-curvature foils. All of these variations are aimed at providing a solution that produces vertical lift, while still resisting side force in stable manner.

Although the foil planform and section are important in the overall design of the foil, both attributes vary little in comparison to the foil profile. The profile of the foil is defined as the projection of the foil onto a plane normal to the free-stream vector, at zero angle of attack. It is common to relate the shape of these different profiles to letters of the alphabet. For example, a constant-curvature-lifting foil, as shown above on the ORMA 60, can be referred to as a C foil. The advantages and disadvantages of different foil profiles are discussed in more depth below.

The simplest way to provide a vertical lift component is by canting a straight foil inboard. The span and cant angle are constrained by any beam restrictions that are in place. This arrangement also reduces righting moment as immersion decreases. Because the vertical lift produced per unit span is constant, a canted foil will provide little heave stability on a fully foiling vessel. This configuration is only useful on very wide platforms with a twin-foil arrangement and is not suited for maneuvering, for example, sailing around a race course with turning marks.

C foils generate most of their vertical lift towards the bottom of the foil curvature when fully lowered. This means the vertical lift generated does not decrease significantly as the immersion ratio decreases, resulting in a foil that will produce lift until it stalls, causing a crash. Because of the constant lift produced, C foils are best suited for foil-assisted craft. C foils and J foils eliminate issues with beam restrictions but have high induced drag once an angle of attack is introduced. Winglets can be added to mitigate this issue, but this significantly complicates the process of retracting the board, and requires complex daggerboard case construction.

An acute L foil is an elegant solution to automatically regulate heave, while using only one foil. As the vessel begins to lift out of the water, the effective span of the vertical strut is reduced. The side force generated by the sails remains constant, so the leeway angle will increase to counter this side force. The induced “slip” increases the pressure on the suction side of the horizontal element, which effectively reduces the angle of attack and the amount of vertical lift produced. This coupling results in a foil that will automatically find an equilibrium immersion ratio, in other words, stable flight. It is important to note that only an acute angle will result in a foil with this form of heave stability; otherwise, an increase in leeway angle will have no effect on the suction side of the horizontal foil. This acute angle also acts as a “safety valve”; as the immersion ratio decreases, the tip of the horizontal element will pierce the free surface and reduce vertical lift regardless of side force. Figure 2 shows the different foil profiles discussed above.

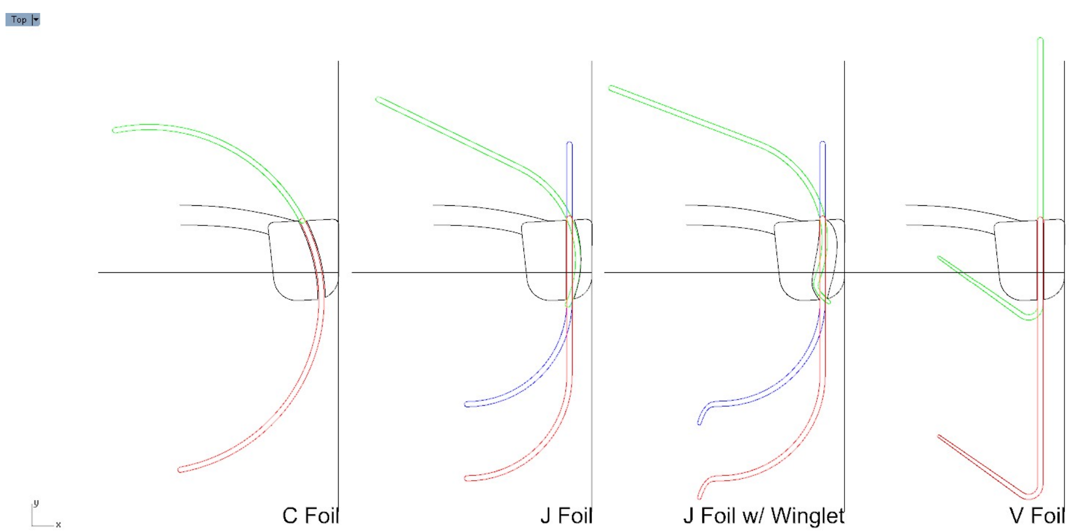

Figure 2. C, J and L-foils
Source: Sailing Anarchy

All of the above components can be combined to suit the application at hand. In particular, one combination, the C-L Foil and its derivatives (shown in Figure 3) have proven to be the most popular. This combination provides heave stability of the acute L configuration with the added benefit of the lift vectoring of the C profile. This setup does lower the righting moment produced by the foil. The righting moment can be improved by adding a point of inflection in the strut of the foil, but this adds complexity to the daggerboard case. Because of its simplicity, as compared to a foil with an inflection point, the C-L foil is the most popular configuration and will be used for our analysis.

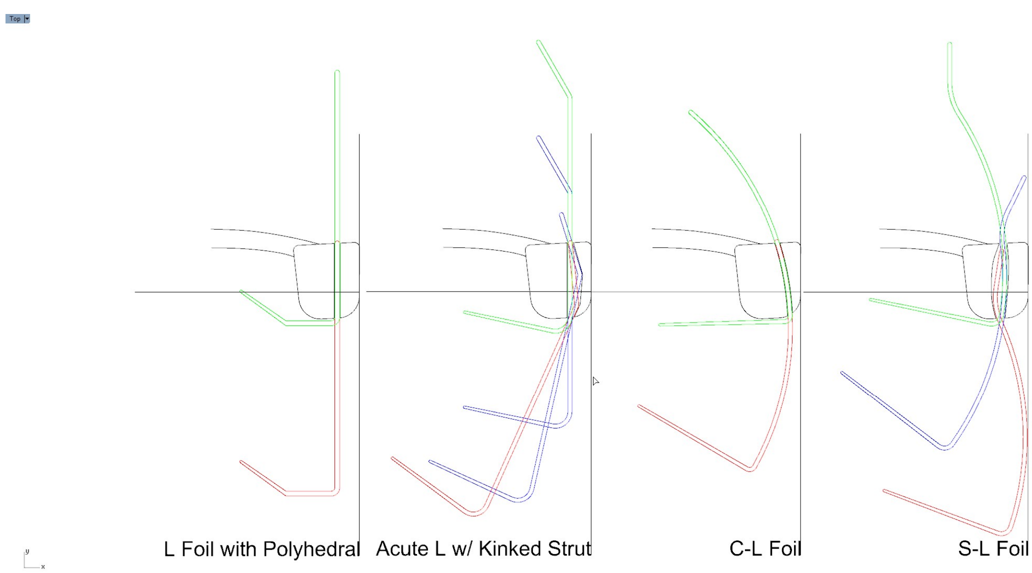

Figure 3 C-L and S-L lifting foils
Source: Sailing Anarchy

DESIGN CONSIDERATIONS

Traditionally, designers have only had to design daggerboards support structure to endure the lateral force produced by the sails, sideforce. However, the addition of a vertical force component, which is often much larger than the sideforce, presents significant design challenges. The additional lifting force not only complicates the design and construction of the foil but also effects the control systems and supporting structure.

Stability

The stability of a foil is just as important as the foil's ability to efficiently produce lift. Lifting foils must be able to produce constant vertical lift while varying speed, leeway angle, pitch angle, heel angle and immersion ratio. The ability to provide constant lift is referred to as heave stability. In addition to heave stability, the lifting foil should also provide some resistance to heel. Modification to foil geometry, in order to improve roll stability, will often result in an increase in drag. This reduction of the lift-to-drag ratio is often necessary to produce a foil that can be used effectively in a racing environment. Although a low drag foil design will produce high peak speeds, a more stable foil design, that is less likely to stall when experiencing minor disturbances will be able to maintain a higher average speed.

Operation

A modern lifting foil is subject to significant hydrodynamic loading. In addition to the stresses experienced during steady state operation, lifting foils are also exposed to significant dynamic loading conditions while maneuvering. The addition of dynamic loads often results in the highest deflections seen by a lifting foil under normal operation. Large deformation of the foil structure may negatively affect the hydrodynamic performance of the foil and in some cases, contribute to stall. This is why it is critical to be able to predict and account for these deflections in the design of a lifting foil.

COMPOSITES

In general, weight savings are of significant importance in any high-performance craft, particularly when foiling is involved. This the main reason that nearly all structural components on fully foiling craft are made using advanced composite materials.

The primary advantage of using composite materials in structures lies in their diversity. A composite structure can be optimized to a much finer degree than other construction methods. Much of this versatility stems from the fibrous nature of FRP materials. Unlike metals and alloys, which have nearly identical material properties in any direction, FRP composites allow for fiber orientation along the axis of highest loading, creating a final structure that has different material properties in each direction. Materials, such as metals, that have constant material properties are known as isotropic materials. If a material's structural properties are different among three mutually orthogonal axis, it is considered orthotropic. By exploiting these properties, an engineer can produce a laminate with specific material properties aligned with load paths. This removal of stiffness, in a direction in which it is not needed, is a way of "trimming fat" from a structure.

In addition to the versatility gained from being isotropic, FRP materials have exceptional structural properties for their weight. The production methods of FRP components also allow for very complex shapes to be created with little effort, as compared to other construction methods. For these reasons, the majority of hydrofoils today are constructed using carbon fiber.

The FEM for the analysis of isotropic materials is well established at this point, with codes capable of solving such problems integrated into most CAE software platforms available today. The accurate simulation of composite materials presents a much more complex problem as a result both of their orthotropic nature and additional failure modes including individual ply failure and delamination. Composite FEA is currently in a phase of development and refinement with only a few software platforms capable of accurately simulating highly refined composite structures.

FOILING YACHTS

In recent years, there have been various methods of utilizing vertical lift producing daggerboards on high-performance sailing craft. Some of the more recent and noteworthy solutions are described below.

AC72

Through a loop-hole in the 2013 America's Cup Class rules, Emirates Team New Zealand was able to design a rule abiding, fully foiling America's Cup Class catamaran in the 34th America's Cup. Other teams were quick to follow this exciting development, marking the birth of the modern AC72 (see Figure 4). Through extensive development, teams were able to create heave-stable foils and complex control systems to establish stable flight.

Figure 4 Full Foiling AC72
Source: sail-world.com

The formal type of racing that occurs in the America's Cup is known as match racing. In match racing, there are two boats which compete head to head in a series of races, with special rules only applicable in the match racing environment. The nature of match racing promotes very close boat-on-boat interactions, which often requires drastic maneuvering. It is in this type of racing that the source of the dynamic forces on lifting foils is most apparent. During these maneuvers it is critical that the foil remain stable in order to prevent collisions or capsize.

IMOCA

The International Monohull Open Class Association (IMOCA) is an organization that organizes the open ocean racing of high-performance, 60-foot monohulls. Historically, this class has been on the leading edge of ocean racing innovation pioneering technologies such as the canting keel, water ballast, and outriggers. Most recently, several IMOCA 60 campaigns have implemented the use of “Dali foils” as seen below in Figure 5. Dali foils resemble the C-V foils used in the America’s Cup except that they are flipped and rotated 90 degrees. The daggerboard’s primary purpose is to provide additional righting moment at high speeds. The additional righting moment allows ballast tanks to be emptied, reducing the craft’s displacement. Additionally, the vertical lift produced to increase righting moment, when combined with the vertical lift produced by an inclined-pivot canting keel, results in a further reduction in displacement.

Figure 5. IMOCA 60 SAFRAN with Dali foils
Source: guillaumeverdier.com

Why FSI?

To date, nearly all published work related to the performance of lifting foils assumes a rigid structure. Assuming a rigid structure greatly simplifies the analysis and still provides a reasonably accurate solution provided structural displacements are small however, a variety of hydrodynamic issues could significantly affect the performance of a flexible daggerboard. Physical conditions such as flutter and cavitation can greatly reduce foil efficiency and may be overlooked without a full FSI analysis.

THEORY

TWO-DIMENSIONAL FOIL CONCEPT

The NACA series of foil sections, originally developed to provide a standard for the design of airplane wings, can be used as a basis for all lifting foil design. The characteristics of a wing, or in this case hydrofoil, may be largely predicted using two-dimensional theory as long as the span is long with respect to the chord, the mach number remains below the subcritical level, and the chordwise velocity is much more significant than the spanwise flow (Abbott, 1959). The sailing hydrofoil satisfies the three previously mentioned criteria. Abbott and von Doenhoff use linear theory to detail two-dimensional foil characteristics based on dimensionless lift and drag coefficients for various foil geometries, and angles of attack. The force-per-unit-span values of lift and drag are given by the following expressions:

$$L' = C_l \frac{1}{2} \rho {V_\infty}^2 c \tag{1}$$

$$D' = C_d \frac{1}{2} \rho {V_\infty}^2 c \tag{2}$$

Potential flow theory does not independently account for the viscous effects that induce separation in flow around a foil section. Without additional corrections, the resulting flow remains attached around the trailing edge at any angle of attack including stall angles, leading to a prediction of zero lift and zero drag, a phenomena known as the D'Alembert paradox. To account for the realistic flow pattern in which the stagnation point is always at the trailing edge, the concept of circulation must be introduced. This is referred to as the Kutta condition, in which sufficient circulation must be developed in order to move the stagnation point to the trailing edge. By integrating the components of pressure normal to the flow over the surface, it can be shown that, regardless of shape, the lift can be predicted using the Kutta-Joukowski theorem.

$$L' = -\rho V_\infty \Gamma \tag{3}$$

THREE-DIMENSIONAL FOIL CONCEPT

Two-dimensional, inviscid foil theory can accurately predict lift and drag for a three-dimensional foil with infinite span and a constant foil section up to the point of stall. Obviously, this approach is not fully applicable to the case of sailing hydrofoil design. Variation in plan form area, foil profile, end effects, and twist, among other three-dimensional aspects significantly alter foil performance, and must be accounted for.

Lifting-Line

The concept of two-dimensional circulation can be extrapolated to three dimensions to predict the variation of lift over the span of a three-dimensional wing that is neglected when using two-dimensional theory. The Prandtl lifting-line theory presents a simplified method to account for this by considering the wing as a straight vortex filament that accounts for the lift inducing circulation as proportional to the strength of the vortex at each point along the filament (Abbott, 1959). Helmholtz's second theorem dictates that a line of vorticity cannot end in a fluid, but must instead be a closed path that extends to the boundary of the fluid. This theorem guides the simplified horseshoe-shaped model, with a constant circulation the length of wing continuing into two trailing vortices extending downstream indefinitely, as seen in Figure 6. To account for the variation in circulation along the span of the foil, as the lift and therefore circulation decreases to zero at the tips, a more complex model superimposing multiple "horseshoe" models can be implemented (Glauert, 1959). See Figure 7.

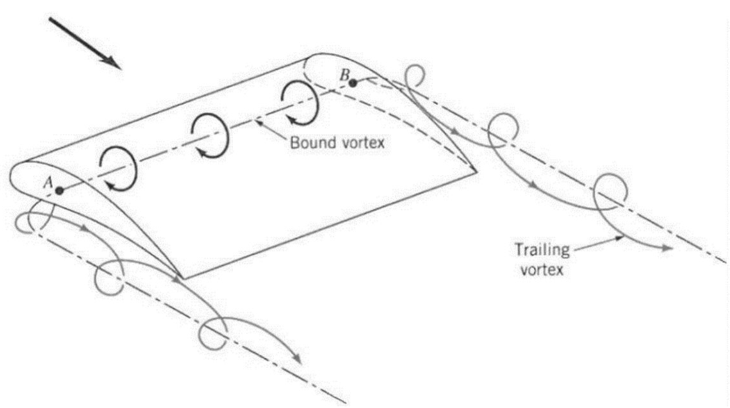

Figure 6. Constant Circulation, Horseshoe Flow Model of Finite Length Wing
Source: Munson

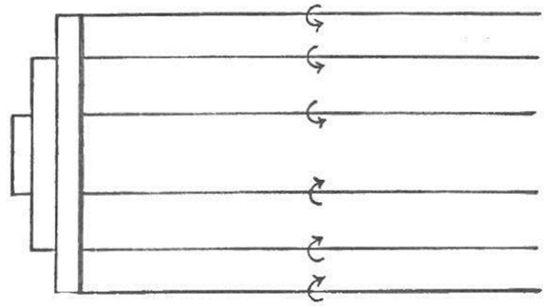

Figure 7. Superimposed Horseshoe Model
Source: Glauert

Induced drag

The flow at any section in a three-dimensional foil varies from that implied by two-dimensional theory, partially from the effects of the trailing vortices. These vortices induce a vertical component of the fluid flow, the downwash velocity w, normal to both the span and the direction of motion, oriented toward the high pressure side of the foil (Glauert, 1959). The impact of this induced flow is to alter the angle of the lift vector towards the drag vector by w/V_∞, adding an element of induced drag, see Figure 8.

.

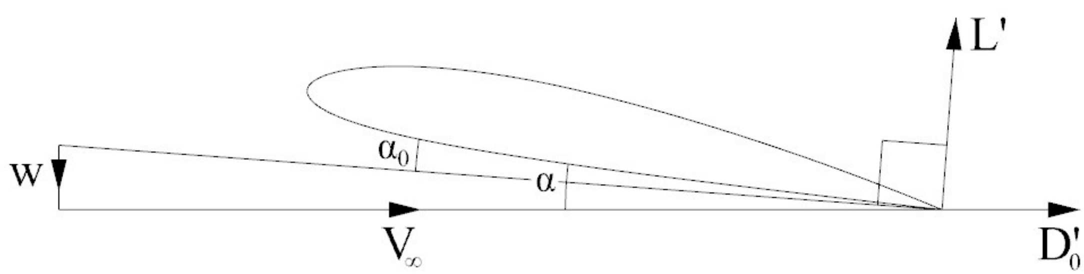

Figure 8: Induced Velocity
Source: Glauert, 1959

Turbulence

Turbulence is defined as a flow regime characterized by unsteady, stochastic or random property changes in which all three velocity components fluctuate around a mean value. Turbulent flow over a lifting surface occurs, in general, at Reynolds numbers above 5×10^6. Turbulent flow is often present close to foil surfaces in the boundary layer. A flow with a turbulent boundary layer can keep the flow attached over a larger percentage of the chord, delaying separation, and thus decreasing pressure drag, at the cost of an increase in skin friction drag. For NACA 6-series foils, pressure drag is always smaller than friction drag, so laminar flow is ideal.

Potential flow theory does not account for viscous effects and therefore must use some form of approximation to account for turbulent effects. As these effects can be very influential on foil performance, Reynolds Averaged Navier Stokes (RANS) CFD programs, which accounts for viscosity, can provide results closer to reality, but requires significantly more computing power.

COMPUTATIONAL FLUID DYNAMICS (CFD)

Three main principles are known to govern fluid dynamics: conservation of mass, conservation of momentum, and conservation of energy. Computational Fluid Dynamics (CFD) solves the RANS equations by applying the above numerically in order to model fluid flow. Star-CCM+ contains a RANSE CFD code that includes the viscosity and vorticity effects neglected by potential flow code.

Reynolds Averaged Navier Stokes Equations

The conservation equations for momentum and mass can be combined and averaged to form the following equation used to solve CFD simulations.

$$\rho\left[\frac{\partial\overline{u_i}}{\partial t}+\overline{u_j}\frac{\partial\overline{u_i}}{\partial x_j}\right]=\rho\vec{g}+\frac{\partial}{\partial x_j}\left[\frac{\partial\bar{p}}{\partial x_i}+\mu\left(\frac{\partial\overline{u_i}}{\partial x_j}+\frac{\partial\overline{u_j}}{\partial x_i}\right)-\rho\overline{u_i{}'u_j{}'}\right] \tag{4}$$

The final three terms, on the right side of the equation, include the pressure gradient, shear stress, and Reynolds stress respectively. Potential flow neglects both shear stress and Reynolds stress and must account for these effects using empirical corrections.

Energy Equation

This physical principal is equivalent to the first law of thermodynamics, which dictates that energy is always conserved. Applying this law to fluid flow, the rate of change of energy inside the element must equal the sum of the net flux of heat into the element, and the rate of work done on the element, from body and surface forces. This law is given by the following equation:

$$\frac{\partial(\rho i)}{\partial t}+\nabla\cdot\left(\rho i\vec{\boldsymbol{V}}\right)=-P\left(\nabla\cdot\vec{\boldsymbol{V}}\right)+\nabla\cdot(k\nabla T)+\varphi \tag{5}$$

where i is the internal energy, P is the absolute pressure, k is the thermal conductivity, T is the temperature, and ψ is the viscous dissipation term. This equation is also presented in its conservative form, for the same reason as the continuity equation.

These two depicted equations, derived from the three classical laws of fluid dynamics, contain six unknowns, ρ, p, u, v, w, i. In order to close the system of equations, the thermal and caloric equations of state are included in the analysis, bringing with them a seventh variable, temperature. These seven equations together provide a problem that can be solved numerically using RANS CFD code.

RANSE Turbulence Models

The numerical discretization of the RANSE requires the use of turbulence models in order to achieve a reasonable computational speed, as the turbulent boundary layer is characterized by unsteady fluctuations. The goal of turbulence modeling is to predict the velocity, pressure, and temperature field without the need to model the entire turbulent flow region (Fast, 2014). This process is achieved through the use of turbulent models offered within various RANS CFD programs. Common models include *k-ε*, *k-ω,* and *SST k-ω*. The *k-ε* model uses a kinetic energy approach and adds relatively little to the computational power required, but does have some shortcomings in more turbulent flows. The *k-ω* model makes use of the transport theorem to apply a specific dissipation rate, however it can require significant additional computing power. The SST *k-ω* model is a combination of both, implementing the *k-ω* model in turbulent boundary layer areas and the *k-ε* model farther from typical turbulent regions (Fast, 2014).

Turbulent Boundary Layer

The boundary layer, is considered to be the thin region near the surface of a body where viscous effects are significant. This layer is necessary for the flow to transition from the free stream velocity outside of the boundary layer to a velocity of zero at the wall. This region is governed by the assumptions that fluid velocity normal to the surface is much less than fluid velocity parallel to the surface, and that the velocity gradient normal to the surface is much higher than that parallel to the surface. Although both laminar and turbulent boundary layer flows share these characteristics, the latter will develop three distinct regions (Figure 9); these include the viscous sublayer, the buffer layer, and the fully turbulent region. The boundary layer characteristics can be described with a near-wall Reynolds number, y+, that is a function of the friction velocity as shown in the flowing equation.

$$y^{+} = \frac{y{*}u_t}{v} \qquad (6)$$

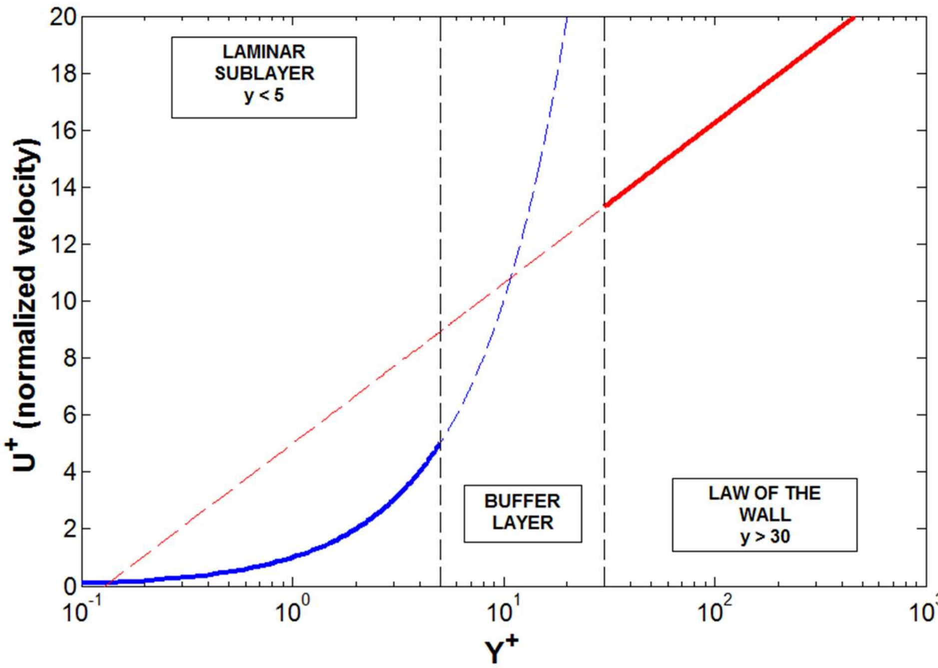

Figure 9 Two-layer zonal approach
Source:www.computationalfluiddynamics.com

Traditional CFD methods have used a wall function approach, where the first cell of the mesh must extend past a point where he y+ value is 50. This approach applies an empirical average without having to precisely solve the viscous sublayer and buffer layer.

The two-layer zonal approach explicitly models these near wall flow effects, requiring significant additional computational time. The *k-ω* turbulence model can simulate both the viscous sublayer and the fully turbulent regions. The first mesh cell must have an outer node y+ value around one with a series of thin growing prism layers for the first ten cells to the extent of the boundary layer.

Boundary Conditions

The previously presented governing equations of CFD apply to all simulations attempted using RANS CFD code. The major difference between the analyses of different physical events lies in the boundary conditions (Anderson 1995). Proper implementation of boundary conditions is necessary in order to obtain accurate numerical simulation results. An example of a boundary condition would be a no slip wall, in viscous flow, where the fluid velocity approaches zero velocity at the wall. These conditions are enabled in simulations to approximate realistic conditions.

FINITE ELEMENT ANALYSIS (FEA)

Finite Element Method

The finite element method provides a numerical, piecewise analytical technique for calculating approximate solutions to problems with irregular or complicated geometry, for which no straightforward analytical solution exists. The method discretizes the continuum of a structural problem into series individual nodes linked by elements. Each node, which may be free in up to six degrees of freedom, acts as a boundary condition for a group of elements, at which point the applied equations must be equal. The elements are assigned an interpolation function, based on the field variable being investigated. The stiffness matrices for each element are combined to produce the matrix defining the entire continuum. Boundary conditions are applied to groups of nodes, and the continuum is then solved for the unknown field variables at the nodal points. Steady problems can be solved using sets of algebraic equations, while unsteady simulations require ordinary differential equations.

The finite element method has gained significant traction, following the growth of computing power, for all forms of solid stress problems and is now viewed as the dominant numerical method in this field. In structural problems, elements are assigned elastic properties with displacement as the unknown field variable.

FLUID STRUCTURE INTERACTION (FSI)

The fluid flow characteristics analyzed in CFD and the structural characteristics modeled in FEA both produce results relevant to many engineering designs. Analyzing the two separately provides the beginning of the design framework however, in many problems the fluid flow can significantly impact the structural response of an object. There are several different methods of Fluid Structure Interaction (FSI) intended to examine different physical phenomena. The breadth of this field of study limits us to discussing just those aspects related to foil design, rather than all possible forms here. The term FSI includes all forms of thermo-mechanical interaction between a solid structure and a fluid. In terms of this thesis, it is the study of the transfer of momentum and forces between a fluid region and a solid body. There are many types of interactions that can be combined to form a multitude of different simulations. A summary of the type of simulation performed in our analysis is shown below in Table 1.

Table 1. FSI Analysis Summary

Motion Specification	**Fixed***
	Free
Structural Response	Rigid
	Deformable*
Coupling Classification	One-Way
	Two-Way*
Coupling Strength	**Strong***
	Weak
Time Domain	**Steady***
	Unsteady

Dynamic Fluid Body Interaction

One of the most basic versions of FSI is dynamic fluid body interaction, DFBI, which occurs when a body is fixed in deformation to examine its movement characteristics through a fluid flow, such as the seakeeping of a ship where the bending of the ship is assumed to not affect the seakeeping characteristics.

Deformable Structure

A flexible structure can be fixed in rotation and translation, but not in deformation. This allows the structure's response to the fluid flow to be examined. This method is applied to the current study in order to examine the structural response of the foil to the encountered fluid flow. A DFBI study can incorporate a deformable structure such as the case in which a ship's structural response in a sea state is examined and correlated to the ship's seakeeping characteristics.

One-way Interaction

One-way interactions can be applied in cases where the structural response will do little to impact the fluid flow. In this case, the forces exerted or heat transferred from the fluid to the structure are applied to the structure, neglecting the impact of the structure's property changes on the fluid flow. A one-way interaction can also be applied in the opposite manner, for example, in a piston and cylinder where the structure impacts the fluid flow, but the flow does little to deform the structure.

Two-way Interaction

Two-way interactions encompass a broad range of FSI simulations. In this type of analysis, the pressures and shear forces from the fluid affect the displacement and deformation of the structure, which in turn affects the fluid flow and therefore the pressures and shear forces that the fluid exerts on the structure. Two-way interactions can be both steady and unsteady, depending on the FSI aspect being investigated.

Weak Coupling

Weak coupling implies that the structural response to the fluid flow is slow. This type of simulation is most often used with stiff structures in compressible flows. Analyses where a steady state response is the target, and the main impacts on fluid flow are from the velocity of the moving structure, are prime candidates for this type of simulation.

Strong Coupling

Nearly incompressible flows, encountering relatively flexible objects, require a strong coupling as opposed to a weak one. These simulations see variations in the flow characteristics from the deformation of the structure, even approaching a steady state solution. Strong coupling is an implicit form of coupling that is necessary for most dynamic problems.

<u>Steady</u>

Steady-state simulations provide a static representation of the impact of fluid flow on a structure, in an attempt to examine the variation in characteristics a steady state, deformed point.

<u>Unsteady</u>

Unsteady simulations are employed to study a variety of dynamic effects. These could include ship motions, flutter in a wing, and other vibrations in a structure.

COMPUTER AIDED ENGINEERING (CAE)

In the modern world, Computer Aided Engineering (CAE) has become the standard for high accuracy engineering analysis. CAE is the broad usage of computer software to aid in an engineering analysis, such as simulation, validation and optimization. Today, there are a variety of CAE packages available to engineers, but most offer the same general functionality with varying degrees of simulation accuracy. It should be noted that most of the CAE software companies issue free or cheap educational licenses which allow students exposure to CAE before entering the professional world.

<u>Composite FEA Analysis</u>

In the initial stages of this thesis, it was determined that the use of composite materials in this analysis was necessary to properly simulate real world deflections. The use of orthotropic materials in composite structures can result in different responses to loading, then comparable isotropic structures. Although the use of orthotropic material properties more closely mimic the real world structures that this thesis is analyzing, it drastically increases the complexity of the analysis. Not only are composite structures made from orthotropic materials, they consist of a combination of different orthotropic materials, each of which has its own material properties. Several CAE codes such as Ansys, Abaqus, and NEi Nastran have recently implemented the functionality to perform simulations on non-isotropic materials, but the results of such analysis is much less validated than typical isotropic simulations.

FSI Coupling

There are several different ways to perform an FSI analysis with CAE. The fluid solver can be run in one code and the solid solver in another and through a method of coupling, a FSI analysis can be run. Most CAE software has the ability to perform some type of coupling with other programs but the level of compatibility differs.

The two most relevant types of coupling are file based coupling and co-simulation. File based coupling (Figure 10) uses output files to transfer data from one code to another. In this process a CFD solution is run, pressure fields and traction fields from this solution are exported from the CFD code and then imported into the FEA code where they are applied to the FE model as loads. This process can be done manually by the user importing and exporting files, or it can be automated with the use of a script. This type of coupling is classified as a weak coupling and is best suited for a one way FSI analysis as the process of iterating is quite cumbersome.

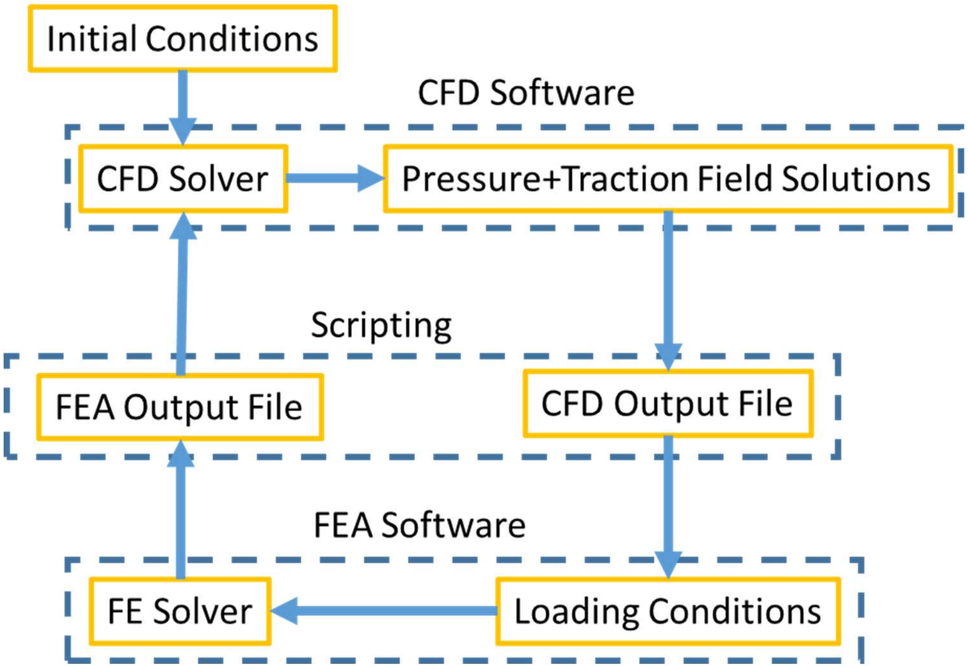

Figure 10. File Based Coupling Workflow

The second type of coupling is known as co-simulation (Figure 11). The main advantage co-simulation is the frequency at which data exchange occurs. A two-way exchange of data forms a deep level of communication between the solvers that makes it possible to simulate the interactions of different physical phenomena. Co-simulation differs from file based coupling in that the coupling between the two codes is much stronger, the exchange of data between the two solvers is done automatically, and the two solvers run simultaneously. This type of coupling is classified as strong coupling and is best applied to a two way FSI analysis.

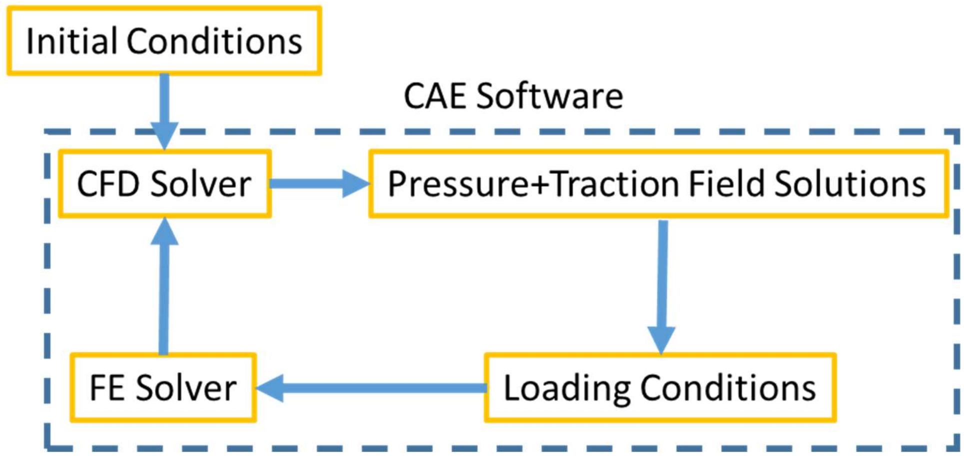

Figure 11. Co-Simulation Workflow

COMPUTATIONAL RESOURCES

When solving an engineering problem with the help of CAE, engineers are very often constrained by the computing power available to them. Multi solver simulations can become computationally expensive very quickly, so many engineers avoid larger, non-linear simulations that could provide higher fidelity insight. To avoid compromising the integrity of such results it is necessary to tailor the solution to the capabilities of the available resources.

High Performance Computing (HPC)

High Performance Computing (HPC) is the use of parallel processing for running advanced applications quickly and efficiently. A decade ago, (HPC) was primarily associated with large supercomputers. Today HPC is available on the entire computer spectrum. More cores per CPU, more and faster memory channels, faster disk storage and faster interconnects have granted wider access of HPC to the general public.

The advent of cloud computing has further broadened exposure to HPC. Cloud computing is the practice of using a network of remote servers to store or process data. Cloud computing access to super computer resources is available to any device capable of connecting to the internet. In the initial stages of this thesis, the use of cloud computing was considered as an option to further expand the computational resources available. This was not deemed necessary with the use of recently acquired computational resources and limited licensing restrictions.

In general, CAE simulation requires large amounts of CPU and RAM to run quickly and efficiently. The number of physical cores and the core clock speed allows trillions of Floating Point Operations (FLOPS) to be performed every second. Modern Intel processors have incorporated an operation called Hyper Threading (HT), which allows the CPU to more evenly distribute the workload among processors. In HT each physical core appears as two virtual cores to the operating system. This increases the number of basic ordered sequences of instructions, threads, that can be passed through a single core, hence the term Hyper-Threading.

Although CPU is the main workhorse in performing numerical calculation, the CPU is fed these calculations by the RAM. For this reason, neither CPU clock speed, nor cache size or even system architecture is as significant as the memory system installed when it comes to simulation performance. Without the proper memory system to support it, large amounts of CPU cannot be properly utilized. The two memory characteristics of interest are the number of channels and memory clock speed. These memory attributes allow the system to keep up with the capacity of the CPU.

PROCEDURE

2D SECTION ANALYSIS

The first step in the design process of a lifting foil is the selection of 2D sections. Analysis of sections in 2D requires much less time and resources than a full 3D analysis, while providing a reasonably accurate prediction of the performance of the lifting foil in the preliminary stage of design.

Hydrodynamic Considerations

From a hydrodynamic standpoint, a section with a high lift to drag ratio and low peak pressure is favorable. A high lift to drag ratio results in lower overall resistance for the lift produced over a range of angles of attack. A lower peak pressure reduces the drag effects caused by separation and cavitation.

In certain operating conditions it is difficult to prevent significant cavitation from occurring. The unsteady dynamic forces and turbulent incident flow experienced by Americas Cup foils make cavitation unavoidable during normal operation. For this reason, some designers have sought out ways to exploit the effects of cavitation. Partial cavitation actually reduces frictional drag, but fluctuations in this area of cavitation usually result in an increase in form drag. Within a range of lift coefficients and cavitation numbers, modifications to the suction side of a section can suppress these oscillations. This beneficial use of cavitation can reduce the frictional resistance of the foil section without the typical increase in form drag.

Structural Considerations

Typically, sections considered for high speed applications are very thin. Often it is necessary to thicken the ideal section once structural aspects are considered. Because the 2D analysis is the very beginning of the design process, the thickness required to limit structural deflections is hard to quantify at this point. Often the initial section thickness is determined using first principles, but this method has its drawbacks, as we will discuss later. Section performance is very sensitive to thickness changes, so the ability to accurately quantify deflections and the subsequent change in performance is critical to the design of a section. This is an example where a FSI analysis can reveal significant attributes of the overall performance of a lifting foil.

Section Selection

The selection of an appropriate 2D section requires a plethora of design considerations as mentioned above, many of which are dependent on the specific vessel characteristics. In order to most accurately simulate the operating conditions experienced during the operation, it was decided to use a section already tailored to this type of application. Morrelli and Melvin Design and Engineering was kind enough to provide the 3D geometry of a CV foil designed for use on an AC50. The local section at the root of the provided geometry was normalized and extracted for use in the 2D analysis. The normalized section can be seen in Figure 12 along with a summary of section characteristics.

Table 2. MM AC50 Section Properties

t_{max}/c (thickness ratio)	=0.14
x_{tmax}/c	=0.35
f_{max}/c (camber ratio)	=0.022
x_{fmax}/c	=0.52

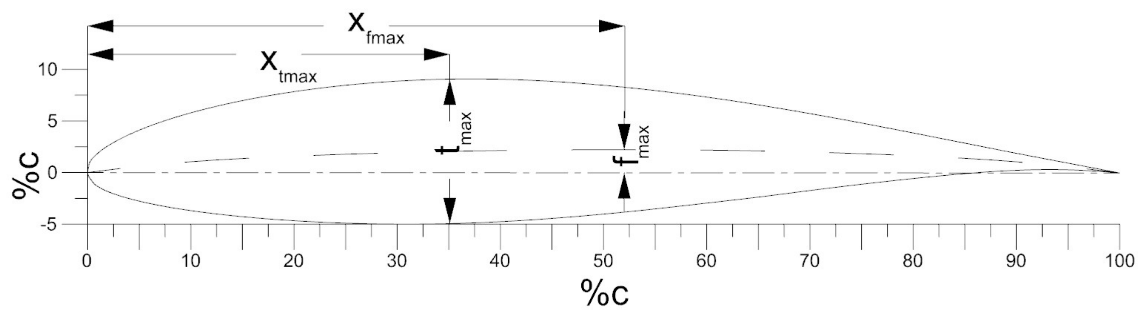

Figure 12. MM AC50 Foil Section

Analysis Limitations

While a 2D analysis is critical to the hydrofoil design process, there are limitations on the results that must be taken into consideration. The most obvious of which is that 2D analysis cannot capture the effects of spanwise flow, which can become significant on complex geometries such as a CV foil. The effects of tip vortices and vortex shedding is not accounted for, as 2D analysis assumes infinite span. These assumptions typically result in an over-prediction of lift/drag characteristics when compared to 3D analysis.

Analysis of this section was performed in XFLR5, a 2D panel code, used for the analysis of airfoil sections at low Reynold Numbers. XFLR5 is simply an open sourced GUI (Graphical User Interface) or “front end” for MIT’s XFOIL code. The code is very robust and has been modified to apply corrections that a typical potential flow analysis would neglect. XFLR5 has the capability to run a corrected viscous and compressible solution, although the models used differ than those used in 3D fluid dynamic simulations.

Analysis Results

The MM AC50 section was tested at three different Reynolds numbers, the same as our 3D testing matrix, over a range of angles of attack. The 2D analysis was performed over a range of α's from -1 degrees to an angle of 15 degrees, just below stall. Although our 3D testing matrix will only cover a fraction of this range of α's, we can more clearly see overall trends with this full range of angles.

The lift to drag ratio of the foil section, as a function of α, is shown below in Figure 13. Here we can see the "efficiency" of the section over the full range of operating conditions. There is a pronounced peak in the lift to drag ratios of each Reynolds number at low α's. This is where the foil is designed to operate for a given speed. This particular thin section has a high lift to drag ratio, but a relatively low angle of stall, characteristics typical of this application. Full results from this analysis are available in Appendix A:.

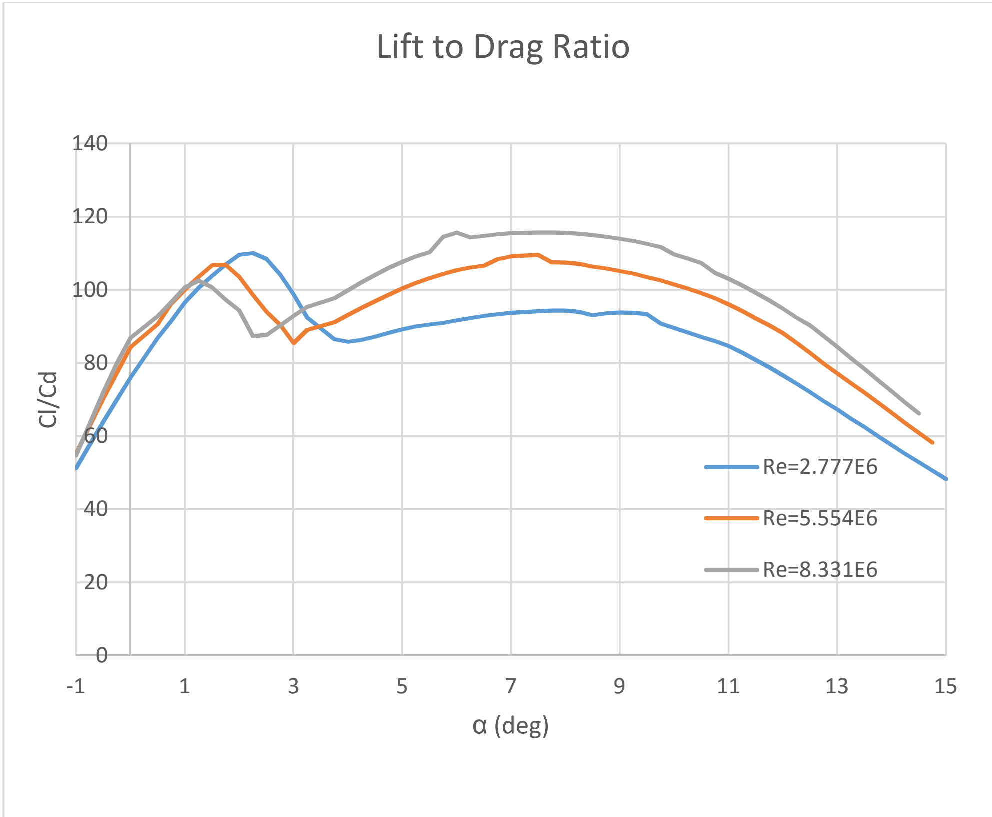

Figure 13. MM AC50 Lift to Drag Ratio

In addition to providing general section performance information, XFLR5 has the capability to show boundary layer thickness along the length of the chord. As can be seen in Figure 14, the boundary layer is the thickest towards the trailing edge of the suction side of the section. The thickness at this location was used to approximate the region where boundary layer effects need to be considered in the 3D analysis.

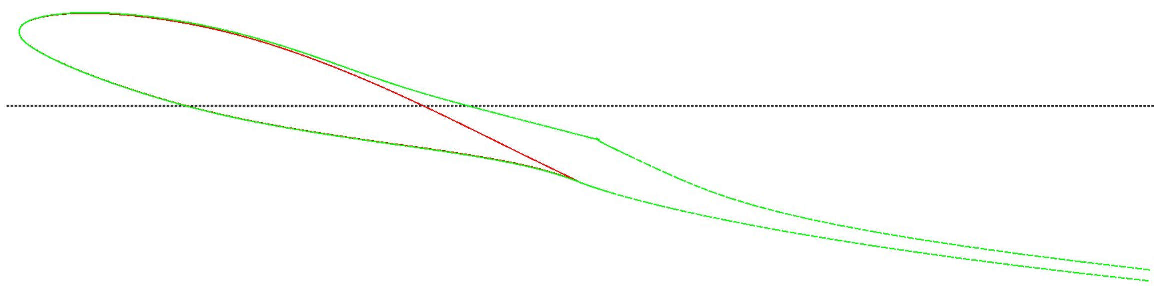

Figure 14 XFLR5 Boundary Layer Output

TEST MATRIX

The Reynolds numbers tested were chosen based on the operating envelope of the geometry provided. A Reynolds number corresponding to fifteen knots was chosen as the low end of our testing matrix to determine the performance of the section at the low end of the foiling envelope. At this point in the operating range we can reasonably assume the vessel is fully foiling and interactions with the hull can be ignored. The upper range of our testing matrix reflects the upper range of speeds experienced by Americas Cup yachts during racing. This is where we can expect the highest deflections and therefore the highest changes in performance.

The 2D results were analyzed to determine the set of α's to be tested. A range of α's from negative one to three degrees was selected. This set of angles is within the drag bucket at all the selected Reynolds numbers, because these angles fall within the desired operating range they are of particular interest in terms of influencing performance. Although high yaw angles, close to stall, will certainly produce the highest deflections, accurately capturing the physical conditions occurring near stall is difficult; additionally, AC 50 catamarans typically operate between -1 degrees and 3 degrees of yaw. For these reason, only the lower end of the possible range of yaw angles was tested (Figure 15)

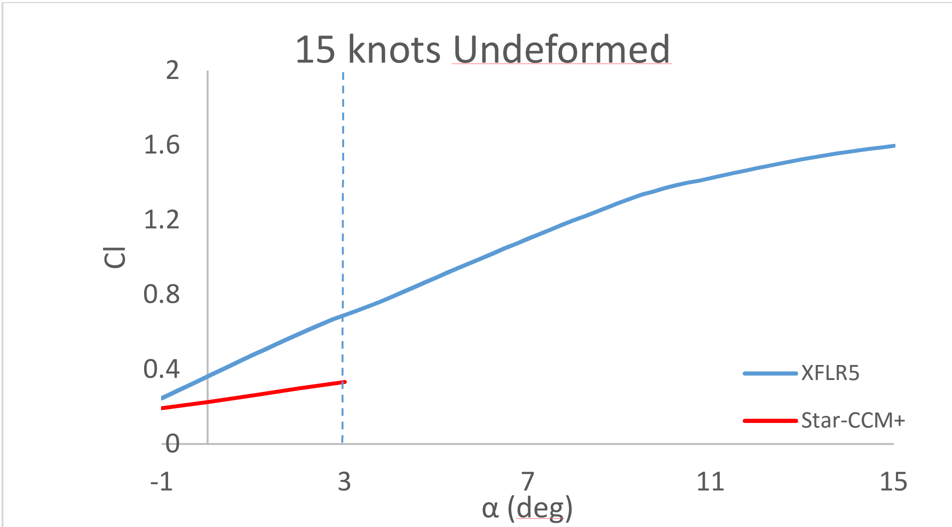

Figure 15. Comparison of Testing Matrix

The final testing matrix is shown in Figure 16, along with a visualization of the parameters varied. The geometry was tested at three different Reynolds numbers over a range of angles of attack from negative one to three degrees. Vertical lift, drag, and side force were then recorded and compared for both the deformed and un-deformed cases. To set the angle of attack, the geometry was rotated about the z-axis. This simulates a change in leeway angle, or yaw, of the vessel. This axis of rotation was selected to induce the maximum possible deflection. All tests were run at an immersion ratio of one to further increase loading.

Testing Matrix	
Speed (kt)	AOA (deg)
15	-1
	0
	1
	2
	3
30	-1
	0
	1
	2
	3
45	-1
	0
	1
	2
	3

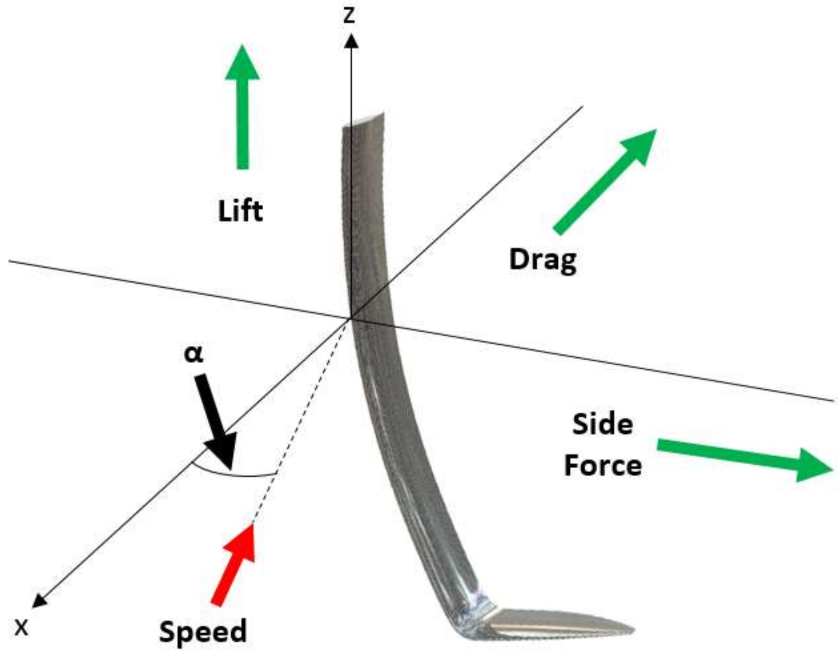

Figure 16. Testing Matrix

SELECTION OF CAE PLATFORM

<u>Star CCM+</u>

Two codes would have to be selected for use in the FSI analysis, a CFD code and an FEA code. Modern CAE software often has these codes integrated under one platform but the robustness of the solvers within each platform varies. From the onset it was clear that CD Adapco's Star CCM+ would be the most practical code to use for our CFD analysis. CD Adapco's (Computational Dynamics-Analysis & Design Application Company Ltd) is a multinational CAE computer software company best known for their CFD products. Additionally, Star CCM+ has been used in previous Webb theses, which provided a baseline procedure for performing marine hydrodynamic analysis.

This left the selection of an FEA solver. Early in the selection process the capability to model orthotropic materials was a consideration in this selection. Out of the solvers available for educational use, two in particular were considered; NEi Nastran and Abaqus. Both of these solvers have the capability to run full FEA on complex composite structures. In the case of NEi Nastran, only file based coupling is possible, which, if used, would effectively limit the FSI analysis to a weak coupling. Abaqus, on the other hand, is a full CAE package and not only has the capability to model composite structures, but is also capable of running FSI co-simulation within itself or coupling with Star CCM+. The biggest issue with both of these options is the associated learning curve. The time spent learning additional software, in addition to the added complexity of a composite structure, was not feasible within the given time constraints.

With the possibility of composite FEA out of the question, Star CCM+ once again became the obvious choice. Similar to Abaqus, Star CCM+ is a full CAE package with the ability to run multiple solvers in the same environment. Although many engineering problems involve fluid dynamics, the real-world solution often involves accounting for a wider range of physical phenomena. For this reason, Star CCM+ has the capability to account for a range of physics, including heat transfer, chemical reaction, combustion, solid transport and acoustics. For this analysis, both the CFD and FEA solver could be run in the same environment. The use of a single simulation package eliminated the need to learn new software and work through any compatibility issues that may be occur in the coupling process.

Another significant benefit from the selection of Star CCM+ as our platform is the customer support and knowledge base offered to users. As an educational user of a CD

Adapco product users are provided with access to a designated customer support representative and to a large database of previous support cases and best practices which proved to be extremely useful.

CD Adapco frequently releases updates to their products, with a new release of Star CCM+ occurring every four months. Of particular interest to this thesis, the January version 11.02 included a fluid structure coupling model. Although the code previously had the capability to perform a FSI analysis, this model automated the nuances involved in the coupling of the FEA and CFD solvers.

Computational Resources Available at Webb

Webb recently acquired two Dell Precision 7910 Towers. These computers have been tailored for use in CAE simulation applications. The general specifications of the tower units are presented below in Table 3. The primary hardware components of interest are the CPU and RAM. These computers have a large number of processors capable of hyper threading, and a high speed memory system, with enough channels to complement the processors.

Examination of previous Webb theses revealed that recent CAE simulation theses were limited by computational resources. This is no longer the case, with the recently upgraded Couch Lab computers. The extra “horsepower” available is especially useful when learning software or troubleshooting simulations. Greater resources allow the solution to develop more quickly and errors to be identified and remedied earlier into a simulation. With these new tower units available, simulation fidelity is now limited by licensing. It is common for the cost of licensing to overcome the cost of physical resources.

Table 3. Couch Lab Resources

Dell Precision Tower 7910		
CPU	Intel Xeon CPU E5-2697 v3	
	Speed	2.60 GHz
	Sockets	2
	Cores	28
	Threads	56
	Scalability	2S

RAM	Installed	192GB
	Speed	2133MHz
	Slots Used	16/16
	Form Factor	DIMM

GPU	NVIDIA Quadro K6000

CPU Study

In general, the more cores available to perform calculations, the faster a CAE simulation can run. This is not entirely true for parallel processing applications. Above a certain number of cores, the time it takes to exchange data between cores becomes greater than the time it would take to process that same data in a single core. This issue is known as scaling or scalability.

In order to best utilize the resources available for this analysis, a CPU study was conducted. Putting all theory aside, this is the best way to gauge system performance. This study was conducted by running the same CFD simulation file to convergence with a varying number of logical processors. The total time to complete 500 iterations was recorded for each case. Results from this study are shown below in Figure 17. Results indicated little benefit from running simulations on more than 10 cores at a time. With a total of 40 licenses available from CD Adapco, this enabled four simulations to be run simultaneously. This is well within the capacity of one the two Couch Lab workstations.

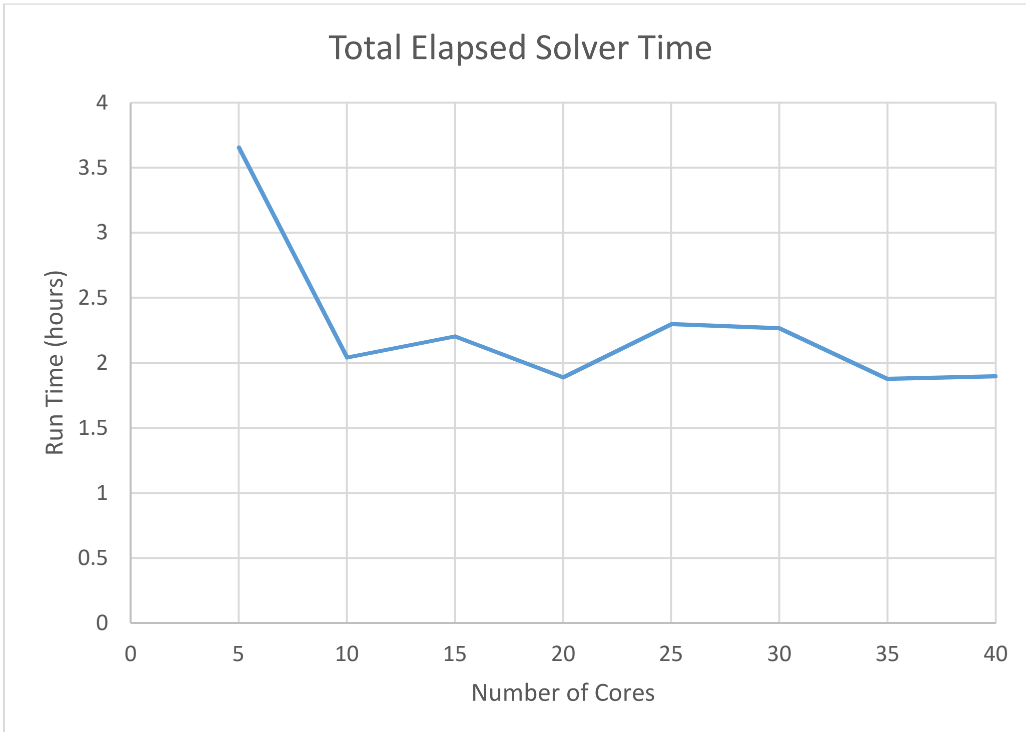

Figure 17 CPU Study Results

COMPUTATIONAL FLUID DYNAMICS

The CFD simulation was first run to convergence independently of the FSI simulation to establish the base characteristics of the undeformed case. This was done for the entire testing matrix. The CFD solution converged after 500 iterations in all cases (Figure 18).

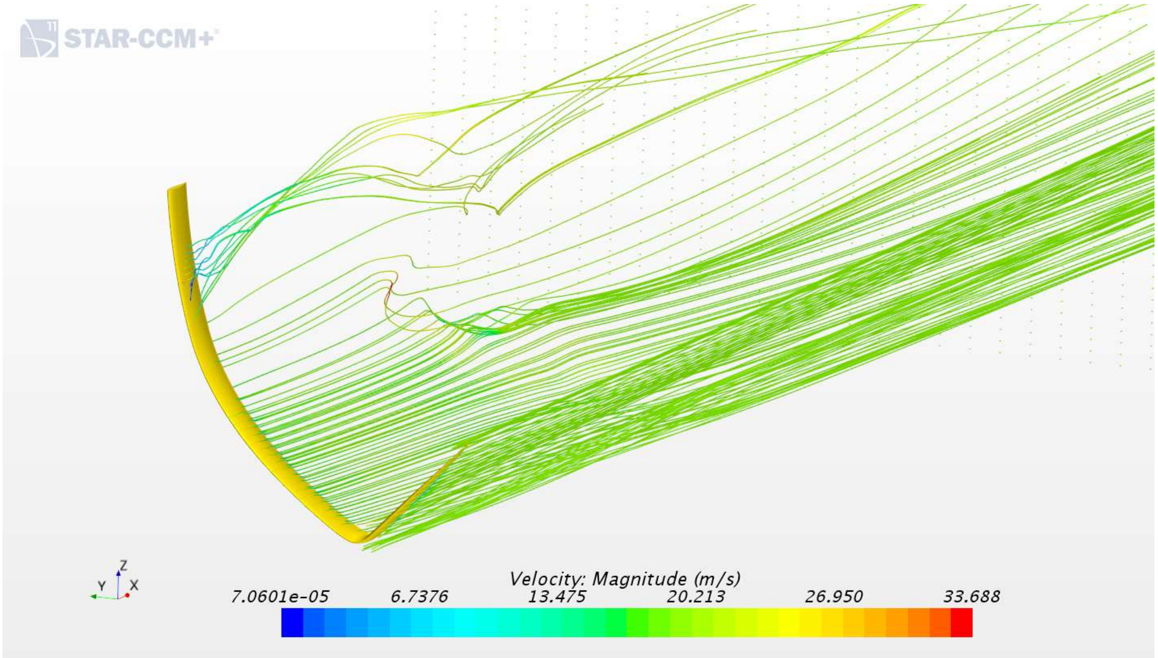

Figure 18 Streamlines Produced from CFD Solution

Geometry

The first step in any multi-physics simulation within StarCCM+ is generating the intended geometry for the study. StarCCM+ has some basic modeling capabilities, but the majority of more complex models will need to be created with a third party CAD program, such as Rhinoceros 3D, which was used for this study. The models can be imported into StarCCM+ using the IGES (Initial Graphics Exchange Specification) format. An important aspect of generating the initial geometry is determining what simplifications, if any, should be applied to the model. This decision should be made based on the computing power available and the level of precision required for design aspects being examined.

A hydrofoil CFD analysis requires the discretization of the foil geometry and the flow domain. The foil geometry is usually imported, while the flow domain can be created in StarCCM+. The flow domain sizing should be large enough to minimize the effect that boundary conditions have on the main region of interest. Adequate flow domain sizing can be established using a mesh sensitivity analysis. This allows an examination of the velocity gradient to ensure that the far field flow is undisturbed by wall effects. It was found that a region sized 16 chord lengths forward and to each side of the foil, 6 chord lengths below, and 40 chord lengths behind the foil was suitable for this simulation (Figure 19).

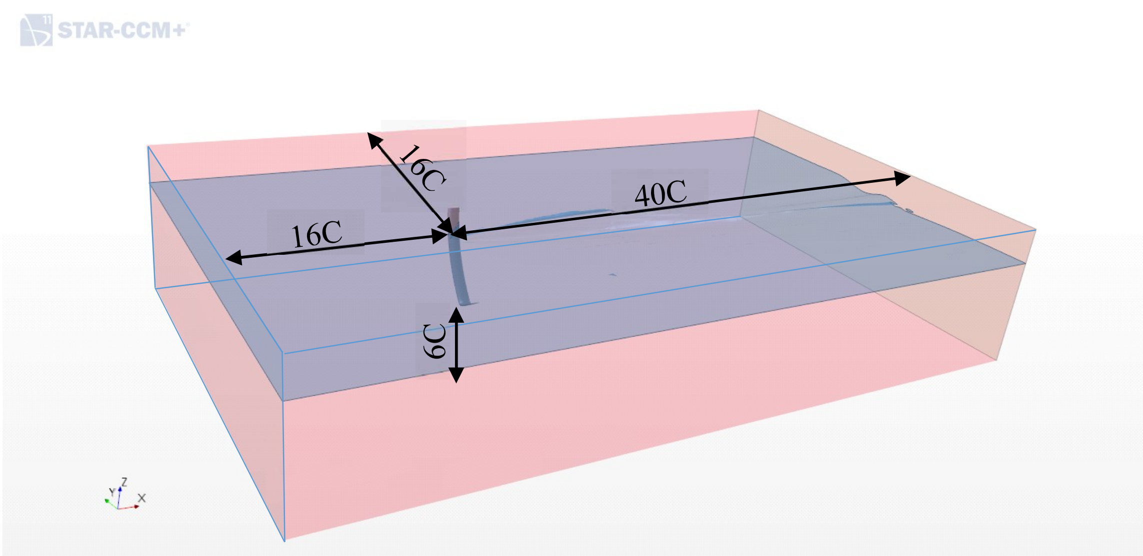

Figure 19. Flow Domain Dimensions

The height of the flow domain above the foil was considered arbitrary as long as it does not affect the free surface, because of the low forces imparted by air in a free surface simulation. Once the two aspects of geometry have been created, the subtract operation can be applied to combine the parts for mesh generation.

Meshing

Proper mesh refinement is crucial in any CFD simulation in order to accurately model the physics being simulated. StarCCM+ has a variety of automatic meshers that can be enabled to generate the volume mesh. The surface remesher, trimmed cell mesher, and prism layer mesher were enabled for this simulation. The surface remesher triangulates the geometry mesh to optimize it for inclusion in the volume mesh. The trimmed cell mesher is a robust and efficient way to produce a predominately hexahedral mesh capable of accepting various user-defined refinements. The prism layer mesher is a supplementary volume mesher that generates orthogonal prismatic cells near walls (Figure 20).

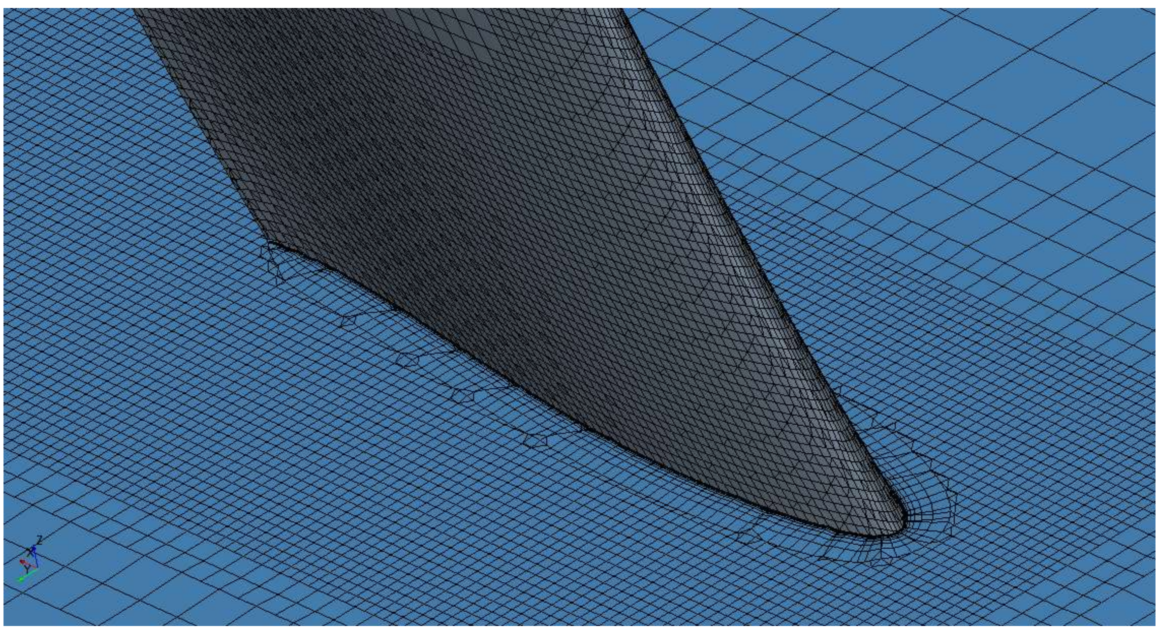

Figure 20. Prism Layer Mesher

The prism layer mesher settings must be applied in conjunction with the turbulence model at the correct y+ values identified to accurately model the boundary layer.

In addition to the surface and volumetric meshers, StarCCM+ has the ability to add custom mesh refinements. These include volumetric refinements (Figure 21a), surface refinements (Figure 21b), wake refinements and others. Volumetric refinements require additional geometry to be generated for such areas as the free surface and foil ventilation region.

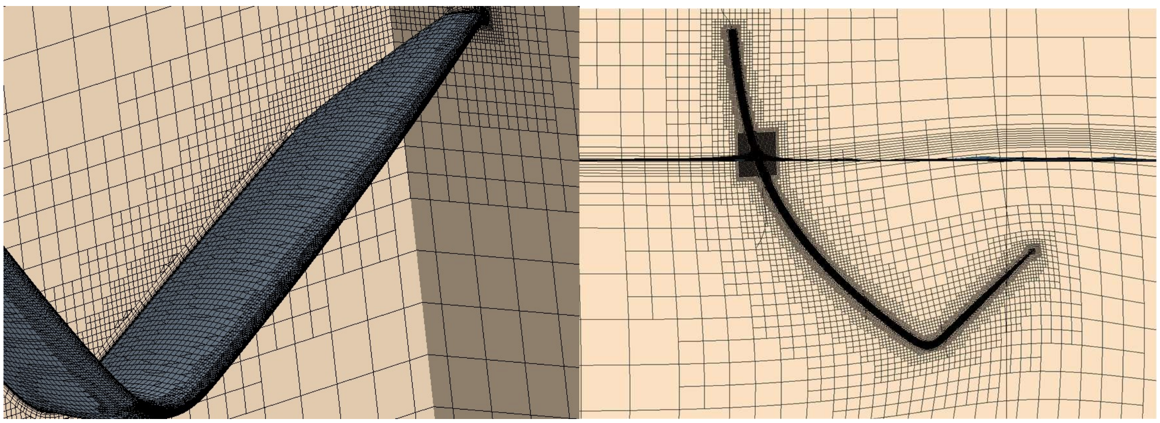

(a) (b)

Figure 21. Surface Refinements (a) and Volumetric Refinements (b)

The wake refinement trimmer (Figure 22) is exceptionally useful in capturing turbulence and vorticity effects downstream of the foil (Figure 23).

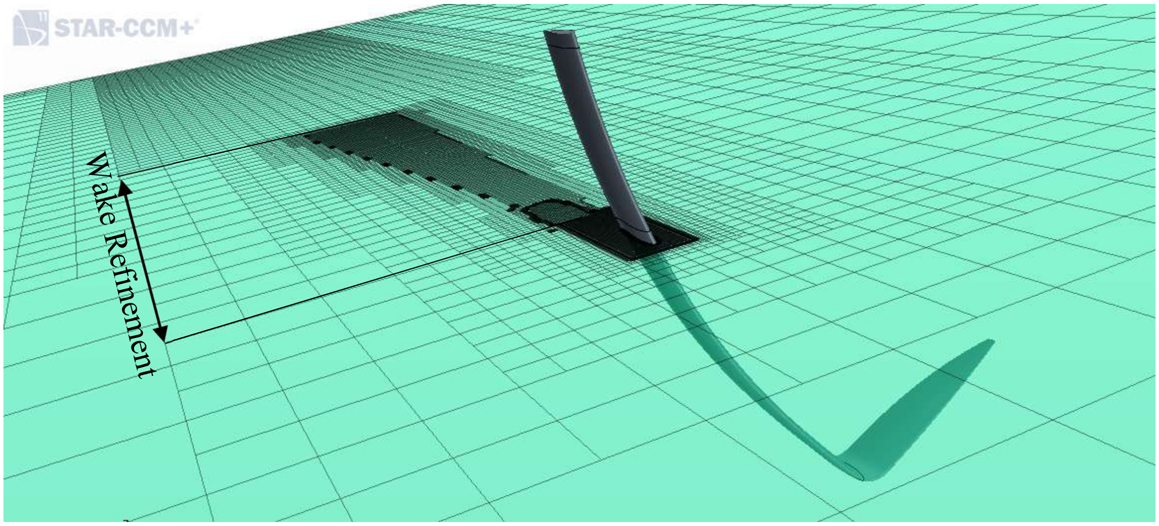

Figure 22. Wake Refinement

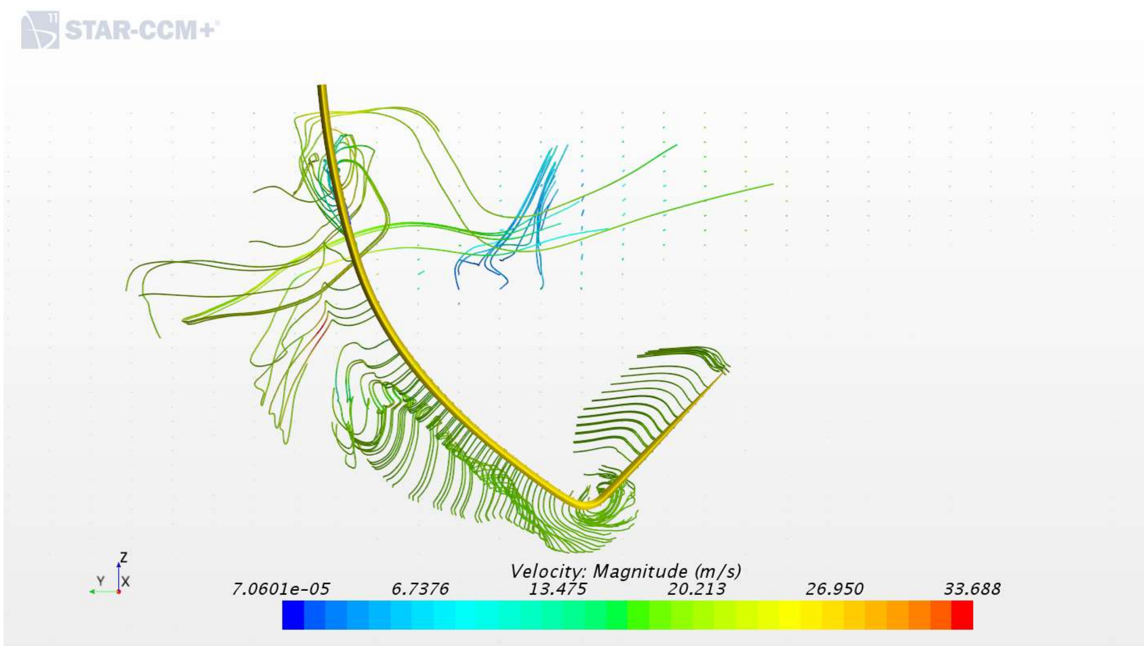

Figure 23 Turbulence Effects

This geometry does not have to be included in the subtract part that represents the extent of the volume mesh, but can be referenced specifically in the mesh custom controls. Surface refinements need to be applied in areas of complex geometry to ensure that mesh simplification does not alter the flow characteristics. Wake regions can be applied to custom surface controls to generate a region of specific size, angle, and refinement relative to a part being analyzed. The exact mesh settings applied for this simulation are outlined in Appendix B:. Once the mesh settings have been applied, the mesh can be generated.

Physics

StarCCM+ offers an extensive range of physics models that can be applied to the simulation continua. The physics models selected apply the proper settings for the intended simulation including single/multiphase flow, heat transfer, solid stress, and aeroacoustics among others. The settings applied dictate the simulation physics within the continua. Various physics options also enable the solvers necessary to converge on that type of solution. The exact physics settings applied for this simulation are presented in Appendix B:. Of particular note for this analysis are models including Reynolds-Averaged Naiver Stokes, k-ε turbulence, Volume of Fluid, and Eulerian Multiphase. The Reynolds-Averaged Naiver Stokes model enables the equations of the same name, described previously in the theory section; these equations consist of the fundamental underlying equations used to govern fluid flow in this simulation. The k-ε turbulence model and its subsequent sub-models are necessary to properly model the turbulent boundary layer flow. The Volume of Fluid model, the Eulerian Multiphase model, along with their respective sub-models, are necessary to model the free surface condition.

Regions

Regions are defined as the connection between the geometric side and physical. The subtract part generated for the flow domain must be assigned to a region prior to generating the mesh, this links the mesh to the appropriate region. The region must then have the proper physics continua applied to it. Regions are used to apply boundary conditions to the problem. The three main boundary conditions for a foil CFD simulation are velocity inlet, pressure outlet, and wall. A velocity inlet is assigned the velocity and angle of the current operating condition being evaluated; in this simulation the front face and the four sides of the flow domain are selected to be velocity inlets. The pressure outlet is assigned the pressure conditions on the outlet face, in this case the back wall of the flow domain. The wall boundary condition is assigned to all parts being analyzed in the simulation, this condition allows shear forces and pressures to be evaluated.

FINITE ELEMENT ANALYSIS

Geometry

Solid stress simulations within StarCCM+ required only the volume of the solid part being analyzed. This can be modeled in a third party CAD software and imported as an IGES file containing the part surfaces. Similar to CFD simulations, the geometry should be carefully refined to balance the computational resources necessary, with the precision level required for the solution being attained.

Meshing

Mesh refinement is as crucial for attaining accurate FEA results as it is for a correct CFD solution. FE mesh refinement is not as critical as the CFD mesh discretization, which requires precise definition for results to be considered accurate (Schwer, 2008). A FE mesh typically features fewer cells than a comparative CFD mesh; in this study the FEA mesh consisted of 1 million cells as compared to the CFD mesh which contains over 6 million cells. The exact mesh settings are presented in Appendix B:. The most course mesh settings determined to produce the same displacement as the theoretical validation in a cantilevered beam case, see Appendix B:, were applied to the foil FE mesh.

Physics

The physics models are chosen in the same manner as the CFD simulation, with implementation of solid stress physics as opposed to fluid flow physics. The main physics model enabled for FEM simulations is the Linear Isotopic Elastic model. This is currently the only form of FEA available within StarCCM+. The isotropic material is also assigned in the physics continua. This is selected under the Solid Model node; for this simulation Aluminum with a Young’s Modulus of 68 GPa was assigned as the material. Additional material properties are provided in Table 4.

Table 4. Aluminum Material Properties

Density	2702 kg/m3
Poisson's Ratio	0.33
Young's Modulus	68 GPa

The Linear Isotropic Elastic model within StarCCM+ only models elastic loading, which means an elastic process with no yield stress limit. The stresses encountered in this study, at the highest speeds, actually exceed the yield stress of aluminum, which is why the majority of actual vertical-lift-producing daggerboards are constructed from orthotropic carbon fiber.

Regions

The regions act in nearly the same manner for FE simulations as for CFD simulations. The parts must first be applied to a region before meshing. Within the regions node, the boundary conditions are applied as segments rather than setting the boundary type. The segments applied include fixed constraints at the top and bottom of the daggerboard trunks, where in typical high performance sailing craft, plastic bushings are installed to allow for daggerboards with different foil sections to be installed.

FLUID STRUCTURE INTERACTION

FSI procedure consists of the method of coupling the CFD and FEM simulations into one. This involves interfacing the two models to converge upon a deformed solution. The mesh, physics, and regions from each can be generated from the same foil geometry in a single simulation file. First the CFD simulation is run on its own to convergence at 500 iterations, set by the stopping criteria, with the FE stress solver frozen. At this point the FE model is coupled with the CFD model through the process depicted in the following section on interfacing, the FE stress solver is unfrozen, and the resultant FSI simulation is run for another 500 iterations to convergence.

Interfacing

Once the CFD and FEA simulations have been completed independently, the rest of the FSI model relies on the coupling of the two. This is accomplished through the use of interfaces in StarCCM+. A couple key operations are necessary to interface the two models. The Fluid Structure Coupling model must be enabled in the solid physics continua. The interface can be generated by multi selecting the two regions and creating an interface between the two. The subtract surfaces from the CFD geometry and the respective part surfaces from FE geometry can be multi selected to create a contact between them. The contacts need to be selected under the interface in order for the solver to run.

Solving

Once the steady, undeformed, solution has developed, the FE solver can be unfrozen and the solution of the FSI problem begins. From this point until the end of the simulation each iteration involves the solution of both the fluid and solid solver. In Figure 24 a visual representation of a two-way FSI algorithm is shown.

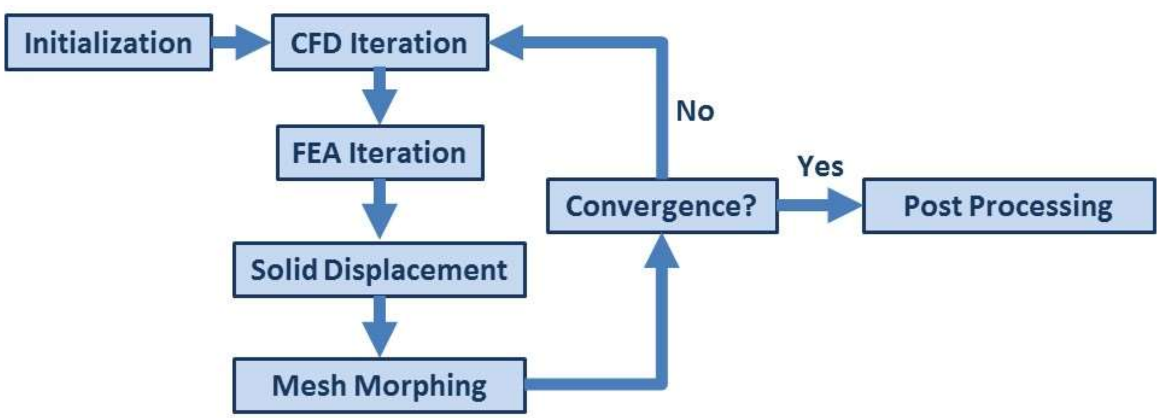

Figure 24 Two-way FSI algorithm

Once both solvers are initialized, a CFD iteration is completed. In co-simulation this first "micro" iteration is known as the leading simulation. The CFD solver produces pressure gradients and traction fields which are then applied as loading conditions to the FE model. The FE model then solves the stiffness matrix for nodal displacements. These displacements are then used by the mesh morpher which distorts the existing CFD mesh to match the solid displacement. A depiction of the displaced FE mesh and morphed CFD mesh can be seen in Figure 25. This process is repeated each iteration until convergence is achieved.

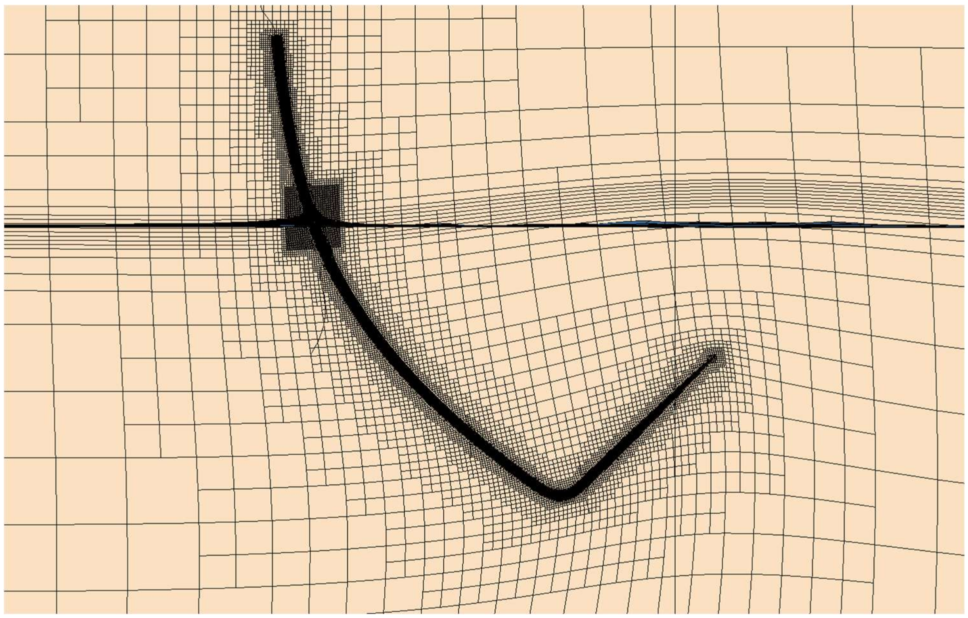

Figure 25. Mesh Morphing

INITIAL CFD SIMULATION

Initial testing consisted of running a series of Star CCM+ environments provided to us by Nate Fast, and running the same foils and testing conditions in the environment that we generated. We compared three yaw angles on the 40-degree tip angle foil and one yaw angle on each of the zero and 20-degree tip angle foils. The results produced in the environment created in the early stages of this thesis were compared to the published results in the Fast (2014) thesis and with the results produced by the Fast simulation files. Overall results from the environment we generated were within ten percent of Fast's published results. This comparison was a form of validation of the Star CCM+ procedure being carried out in the initial stages. This exercise also helped with the familiarization of Star CCM+ and its workflow. The results from this validation can be seen in Appendix C.

RESULTS

Testing was completed for both the undeformed foil, with a solely CFD simulation, and for the deformed foil, with coupled CFD and FEA within StarCCM+, over the entire testing range. The undeformed results, presented below in Figure 26, show increasing vertical lift, sideforce, and drag with increasing α and faster operating speeds. The full results can be found in Appendix E. This increase in lift and sideforce can be attributed primarily to the lower pressure developed on the suction side the foil at higher speeds. (Appendix E).

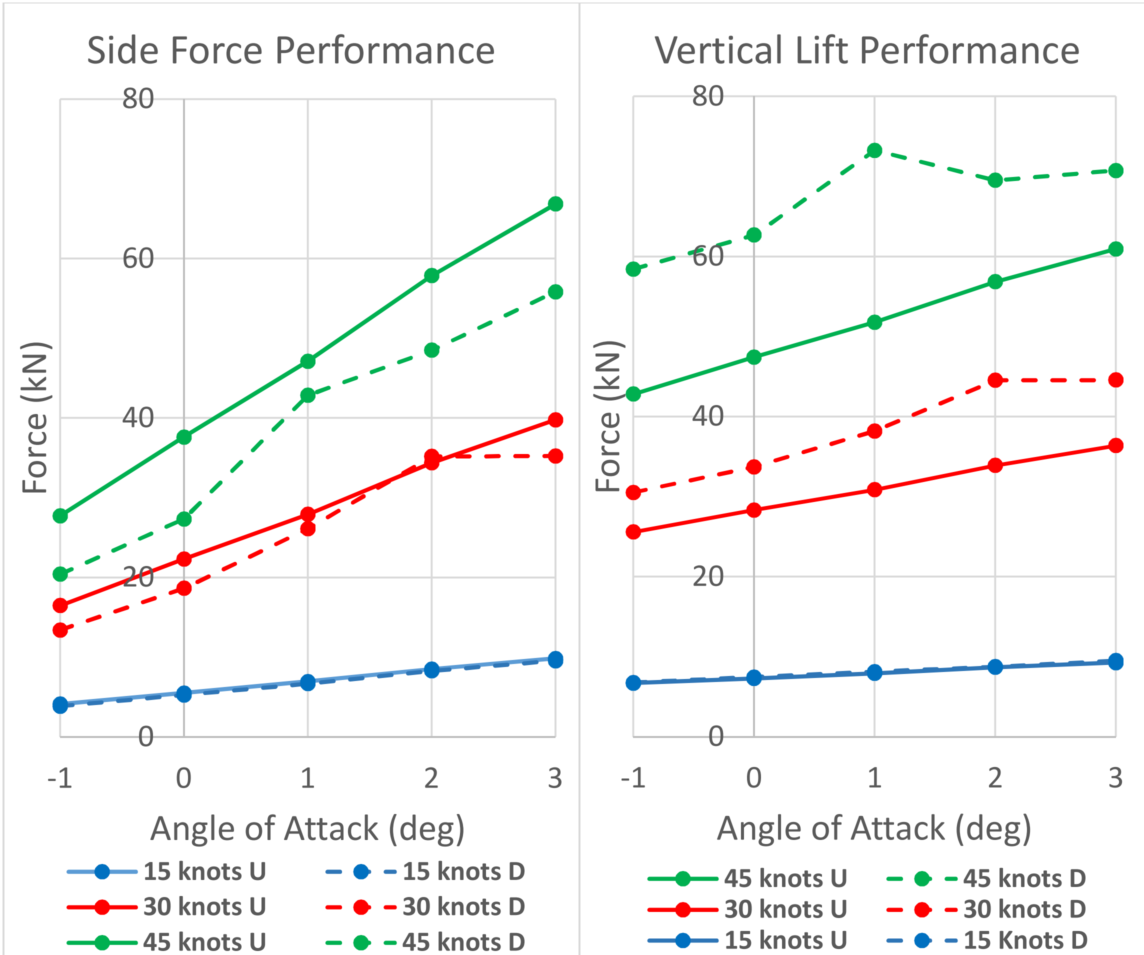

(a) (b)

Figure 26 Side Force Results (a) and Vertical Lift (b)

These findings agree with those produced in past Webb CFD theses. The deformed case at 15 knots had very little significant variation from the undeformed case at the same speed. This correlates with the low forces produced at the lowest tested operating speed of 15 knots.

As the foil begins to deform, the projected area in the lateral plane, roughly proportional to the sideforce produced, decreases, while the vertical area, likewise proportional to vertical lift, increases. The findings at both 30 and 45 knots show a decrease in sideforce (Appendix E) and an increase in lift in the deformed case. This agrees with the expected results from the variance in projected area. The highest operating speed of 45 knots produced the most significant changes in deformed performance (Figure 27). An interesting point to note in the results graph is where the sideforce increases, for the deformed case, at 30 knots and a two degree angle of attack. This does not correlate with the change in projected area. Further investigation is needed to determine the cause and possible benefit in that operating region.

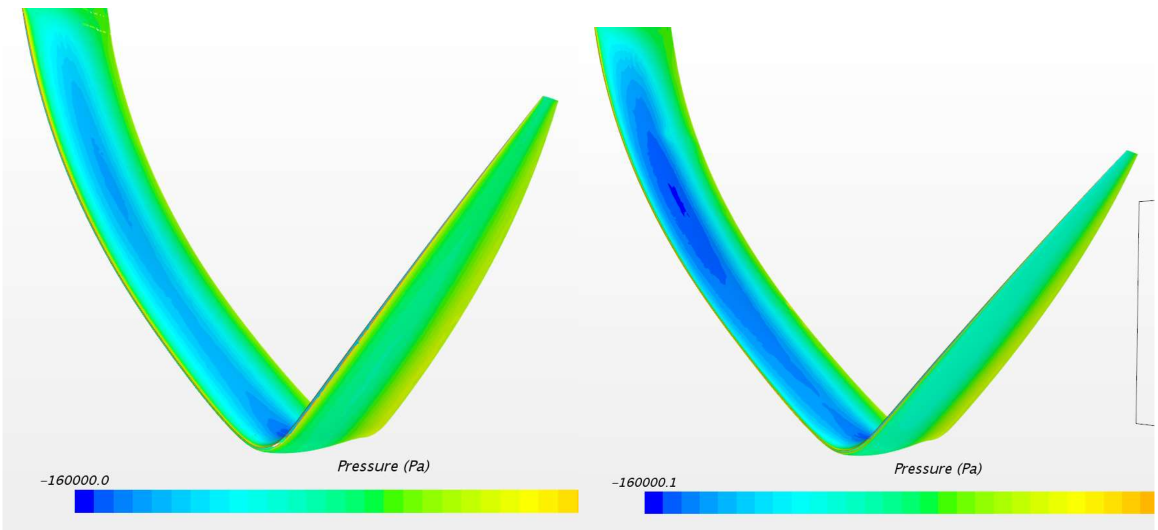

(a) (b)

Figure 27. Pressure gradient developed at $\alpha = -1°$ (a) and $\alpha = 3°$ (b) at 45kts

The lift to drag ratio was established using the total resultant force of the vertical lift and sideforce generated and the expanded area as the reference area. Once again, the 15 knot case varied little from an undeformed to deformed case. The 30 and 45 knot cases were found to have significant decreases in lift to drag ratio at α's of over 2 degrees from the undeformed case to the deformed case.

The deformation correlated with a cantilevered beam, with a maximum deflection at the tip of the foil. The difference in deflections as a result of varying angle of attack can be seen in Figure 28.

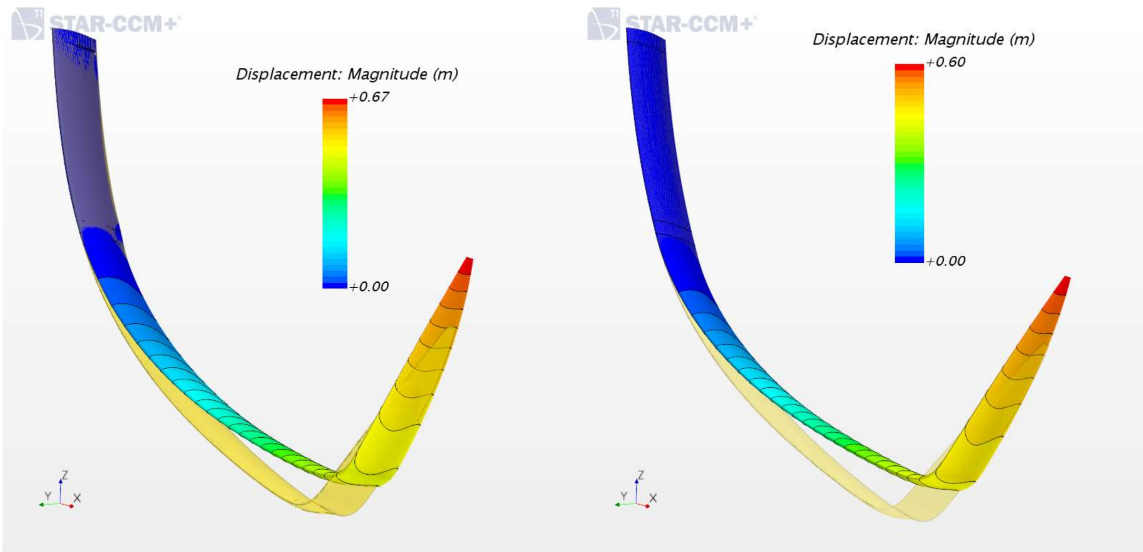

Figure 28 Displacement at α = -1° (a) and α = 3° (b) at 45kts respectively

Likewise, the stresses reached a maximum at the fixed constraint of the daggerboard trunk (Figure 29), on the low pressure inboard side of the foil, farther from the neutral axis. The aluminum's ultimate yield strength was exceeded in some of the higher loading conditions.

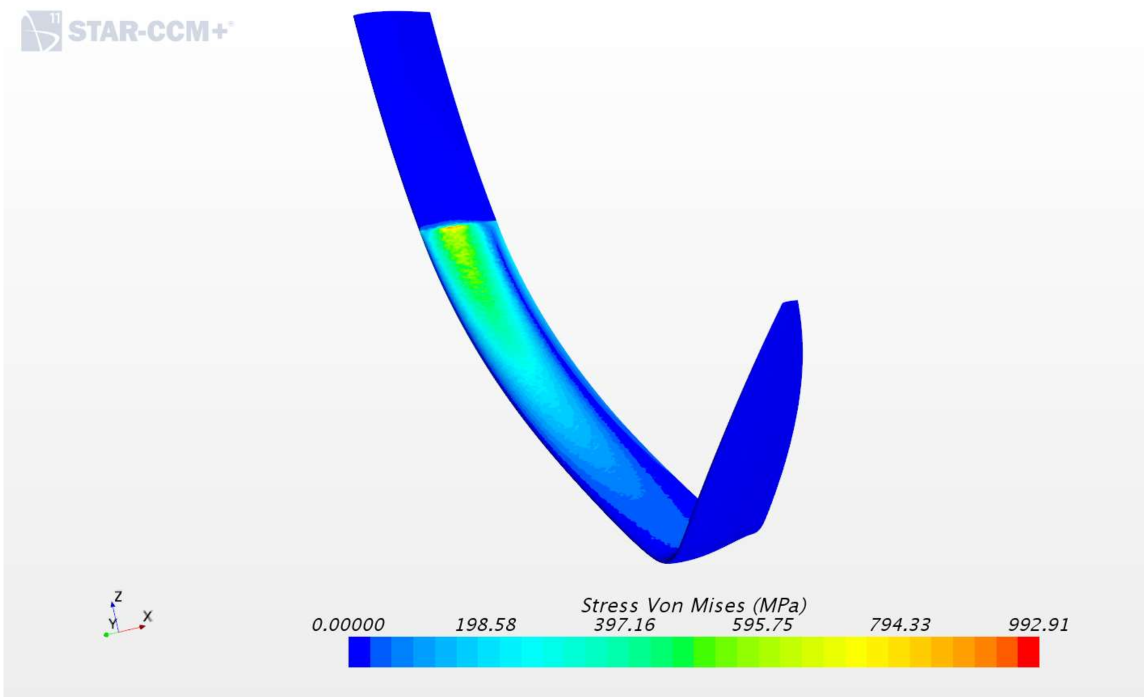

Figure 29 Von Misses Stress at 45kts, α = 3°

CONCLUSION

The main objective of this thesis is to couple a CFD analysis and a FE analysis, in order to complete a FSI study of a C-V hydrofoil. A powerful fluid structure interaction analysis procedure was created within the Star-CCM+ environment. The simulation created was tested through a variety of operating conditions, and provided results that can be useful in a preliminary analysis with promising results. Vertical-lift and side-force results follow deformed changes in projected area as expected. Although validation with experimental data is difficult to perform due to the proprietary nature of this work, it is a first step forward in understanding the difference between a pure CFD analysis and FSI analysis.

A secondary goal of this thesis is to evaluate the necessity of considering fluid structure interactions through comparison of a non-deformable CFD analysis to the FSI results. Deformation was found to significantly impact foil performance at speeds of 30 knots and above. As boats using these foils typically operate in the 40 knot plus range, the necessity of including this form of analysis for America's Cup boats and other high speed foiling craft is apparent. Boats that use non-vertical-lift-producing daggerboards, and do not exceed 15 knots, would likely not benefit greatly from this type of analysis.

RECOMMENDATIONS FOR FUTURE WORK

This thesis builds on past Webb Institute CFD theses on foils, implementing the same style of foil and adding an FEA of the structure to examine the effects of deformation on hydrodynamic performance. These prior theses provided useful stepping stones for the work presented here, just as this work has potential to foster future theses in this field.

A major simplification was made in this study in the use of isotropic aluminum, as opposed to the orthotropic carbon fiber laminates that are typically used for foil construction. StarCCM+ does not currently contain an orthotropic FE solver, but is currently working on implementing one to be released in the near future. A continuation of this work could incorporate the more realistic aspects of composite construction, either within StarCCM+ if possible, or by coupling StarCCM+ with an independent FE solver such as ABAQUS, one of the current leaders in composite FEA.

The modeling of cavitation on slender bodies with high Reynolds numbers is a field currently at the leading edge of research. Although not modeled in this analysis, areas of potential cavitation can be visualized by defining an isosurface capturing pressures below the saturation pressure of water. Areas where cavitation is likely to occur in this analysis can be seen below in Figure 30.

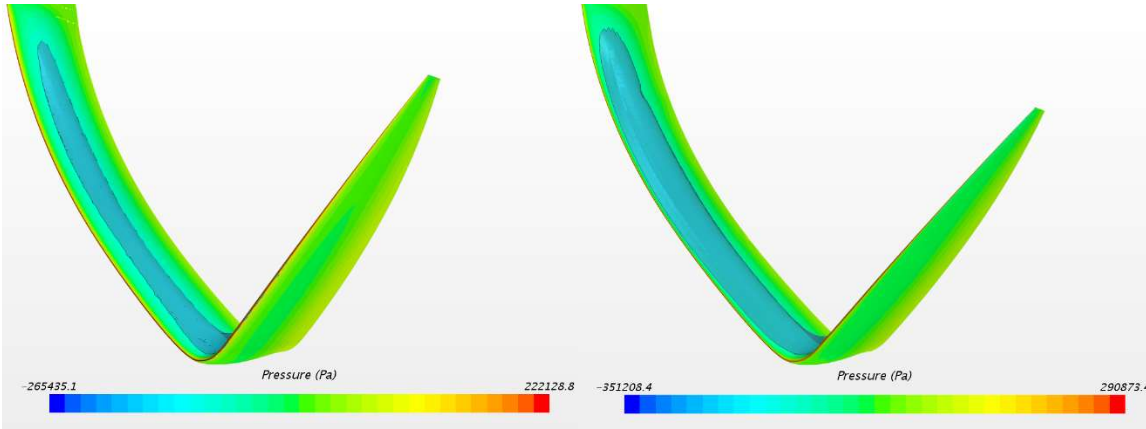

Figure 30. Regions where onset of cavitation is possible

Cavitation modeling requires significant computing power and complex meshing schemes. This work established regions of possible cavitation on the low pressure side of the C strut of the C-V foil at 45 knots that increased in size with greater angles of attack. As foils reach faster and faster speeds, cavitation will become unavoidable and will need to be integrated into the design of high speed foils. The modeling of cavitation within StarCCM+, in regard to high speed foils, could provide an interesting avenue for future research.

This study neglected unsteady flow effects, and primarily focused on converging on a steady state deformed solution. Many unsteady flow effects occur in the real world and merit future investigation. Flutter in the foil can greatly impact the hydrodynamic performance attributes. Vibration modes in the foil can significantly impact the structural response and failure modes of the foil. Further work incorporating unsteady effects will become more reasonable as computing power increases.

The goal of this thesis was to establish a working FSI analysis procedure for vertical-lift-producing daggerboards. This study was completed using a single geometry. The procedure could be implemented to optimize a foil for a particular design condition, either through a FSI study of a systemic series of foils or through coupling StarCCM+ with an optimization software such as Caeses or the Optimate module integrated into StarCCM+.

LIST OF REFERENCES

Abbot, Ira H. and Albert E. von Doenhoff. *Theory of Wing Sections*. New York: Dover Publications, 1959.

Fast, Nathan. *A Computational Fluid Dynamics Analysis of Vertical-Lift-Producing Daggerboards for High-Performance Sailing Yachts*. Glen Cove: Webb Institute, 2014.

Fossati, F. (2007). Aero-Hydrodynamics and the Performance of Sailing Yachts. Milano:Polipress-Politecnico.

Glauert, H. *The Elements of Aerofoil and Airscrew Theory*. Cambridge, UK: University Press, 1959.

Larsson, L., & Eliasson, R. E. (1994). Principles of Yacht Design. Camden, Maine:McGraw-Hill.

Munson, B., D. Young and T. Okiishi. *Fundamentals of Fluid Mechanics*. Hoboken: John Wiley & Sons, 2006.

Schacht, Roxanne and Doug Zangre. *A Computational Fluid Dynamics Analysis of Curved Daggerboards on High Performance Sailing Yachts*. Glen Cove: Webb Institute, 2013.

Schwer, Leonard E. (2008). *Is Your Mesh Refined Enough? Estimating Discretization Error using GCI. Proc. LS-DYNA.* Anwenderforum, Bamberg, 1-1-45.

APPENDIX A: 2D SECTION ANALYSIS RESULTS

2D SECTION ANALYSIS RESULTS

The following plots show the hydrodynamic properties of interest of the FastThesis01 Section. Lift and moment coefficient as a function of angle of attack is shown in the two plots below. The maximum coefficient of lift and angle of attack at which this occurs can be seen in the preceding table.

Summary of 2D Section Analysis Results

Bold values indicate ones used in our 3D test matrix.

Re ($x10^{-6}$)	**2.777**	**5.554**	**8.331**	**2.777**	**5.554**	**8.331**
α(deg)	**CL**			**L/D**		
-1.00	**0.25**	**0.25**	**0.25**	**51.28**	**55.33**	**54.74**
-0.75	0.28	0.28	0.28	57.71	62.89	63.47
-0.50	0.30	0.31	0.31	63.98	70.37	72.02
-0.25	0.33	0.34	0.34	70.05	77.42	80.08
0.00	**0.36**	**0.37**	**0.37**	**75.93**	**84.37**	**86.90**
0.50	0.42	0.40	0.40	86.83	90.62	92.83
0.75	0.45	0.42	0.42	91.60	96.29	96.71
1.00	**0.48**	**0.45**	**0.45**	**96.58**	**100.04**	**100.69**
1.25	0.51	0.48	0.48	100.51	103.59	102.54
1.50	0.54	0.51	0.51	103.81	106.71	100.69
1.75	0.56	0.54	0.53	106.98	106.82	97.29
2.00	**0.59**	**0.56**	**0.56**	**109.59**	**103.55**	**94.36**
2.25	0.62	0.59	0.61	110.01	98.56	87.27
2.50	0.64	0.61	0.63	108.45	94.07	87.69
2.75	0.67	0.63	0.66	104.19	90.41	90.26
3.00	**0.69**	**0.66**	**0.69**	**98.77**	**85.43**	**92.92**
3.25	0.71	0.71	0.72	92.42	89.03	95.33
3.75	0.76	0.74	0.74	86.55	91.12	97.72
4.00	0.79	0.77	0.77	85.79	93.13	99.94
4.25	0.81	0.80	0.80	86.31	95.06	102.11
4.50	0.84	0.82	0.83	87.18	96.90	104.10
4.75	0.87	0.85	0.86	88.24	98.72	105.99
5.00	0.89	0.88	0.88	89.19	100.40	107.65
5.25	0.92	0.91	0.91	89.98	101.91	109.15
5.50	0.95	0.93	0.94	90.58	103.25	110.34
5.75	0.97	0.96	1.02	90.97	104.38	114.48
6.00	1.00	0.99	1.05	91.67	105.39	115.66
6.25	1.02	1.01	1.07	92.32	106.15	114.33

Re (x10^{-6})	2.777	5.554	8.331	2.777	5.554	8.331
α(deg)	**CL**			**L/D**		
6.50	1.05	1.04	1.10	92.93	106.65	114.78
6.75	1.07	1.09	1.13	93.33	108.39	115.22
7.00	1.10	1.12	1.15	93.70	109.16	115.45
7.50	1.15	1.14	1.18	94.15	109.56	115.62
7.75	1.17	1.17	1.20	94.32	107.49	115.63
8.00	1.20	1.19	1.23	94.29	107.46	115.53
8.25	1.22	1.24	1.25	93.92	107.12	115.31
8.50	1.24	1.29	1.28	93.09	106.38	114.97
8.75	1.27	1.31	1.30	93.64	105.83	114.56
9.00	1.29	1.34	1.33	93.81	105.18	113.98
9.25	1.32	1.36	1.35	93.69	104.41	113.36
9.50	1.34	1.38	1.37	93.33	103.53	112.58
9.75	1.35	1.40	1.40	90.78	102.58	111.75
10.00	1.37	1.43	1.44	89.56	101.52	109.74
10.25	1.39	1.45	1.46	88.38	100.35	108.61
10.50	1.40	1.46	1.48	87.11	99.08	107.36
10.75	1.41	1.48	1.52	85.96	97.69	104.59
11.00	1.42	1.49	1.54	84.72	96.05	103.05
11.25	1.44	1.51	1.55	82.86	94.18	101.23
11.50	1.45	1.52	1.56	80.87	92.18	99.24
11.75	1.47	1.53	1.58	78.78	90.24	97.10
12.00	1.48	1.54	1.59	76.59	88.20	94.80
12.25	1.49	1.55	1.60	74.33	85.53	92.47
12.50	1.50	1.56	1.61	72.02	82.75	90.30
12.75	1.51	1.57	1.62	69.65	79.88	87.39
13.00	1.53	1.58	1.63	67.26	77.16	84.40
13.25	1.54	1.59	1.64	64.84	74.55	81.39
13.50	1.55	1.61	1.65	62.41	71.89	78.35
13.75	1.56	1.62	1.66	59.98	69.18	75.28
14.00	1.57	1.63	1.67	57.57	66.42	72.25
14.25	1.57	1.63	1.68	55.19	63.63	69.24
14.50	1.58	1.64	1.69	52.84	60.89	66.24
14.75	1.59	1.65		50.54	58.22	
15.00	1.60			48.29		

Re ($x10^{-6}$)	2.777	5.554	8.331
Cd	Cl		
0.005	0.25	0.25	0.25
0.005	0.28	0.28	0.28
0.005	0.30	0.31	0.31
0.005	0.33	0.34	0.34
0.005	0.36	0.37	0.37
0.005	0.42	0.40	0.40
0.005	0.45	0.42	0.42
0.005	0.48	0.45	0.45
0.005	0.51	0.48	0.48
0.005	0.54	0.51	0.51
0.005	0.56	0.54	0.53
0.005	0.59	0.56	0.56
0.006	0.62	0.59	0.61
0.006	0.64	0.61	0.63
0.006	0.67	0.63	0.66
0.007	0.69	0.66	0.69
0.008	0.71	0.71	0.72
0.009	0.76	0.74	0.74
0.009	0.79	0.77	0.77
0.009	0.81	0.80	0.80
0.010	0.84	0.82	0.83
0.010	0.87	0.85	0.86
0.010	0.89	0.88	0.88
0.010	0.92	0.91	0.91
0.010	0.95	0.93	0.94
0.011	0.97	0.96	1.02
0.011	1.00	0.99	1.05
0.011	1.02	1.01	1.07
0.011	1.05	1.04	1.10
0.012	1.07	1.09	1.13
0.012	1.10	1.12	1.15
0.012	1.15	1.14	1.18
0.012	1.17	1.17	1.20
0.013	1.20	1.19	1.23
0.013	1.22	1.24	1.25
0.013	1.24	1.29	1.28
0.014	1.27	1.31	1.30
0.014	1.29	1.34	1.33
0.014	1.32	1.36	1.35

Re ($x10^{-6}$)	2.777	5.554	8.331
Cd	**Cl**		
0.014	1.34	1.38	1.37
0.015	1.35	1.40	1.40
0.015	1.37	1.43	1.44
0.016	1.39	1.45	1.46
0.016	1.40	1.46	1.48
0.016	1.41	1.48	1.52
0.017	1.42	1.49	1.54
0.017	1.44	1.51	1.55
0.018	1.45	1.52	1.56
0.019	1.47	1.53	1.58
0.019	1.48	1.54	1.59
0.020	1.49	1.55	1.60
0.021	1.50	1.56	1.61
0.022	1.51	1.57	1.62
0.023	1.53	1.58	1.63
0.024	1.54	1.59	1.64
0.025	1.55	1.61	1.65
0.026	1.56	1.62	1.66
0.027	1.57	1.63	1.67
0.029	1.57	1.63	1.68
0.030	1.58	1.64	1.69
0.031	1.59	1.65	
0.033	1.60		

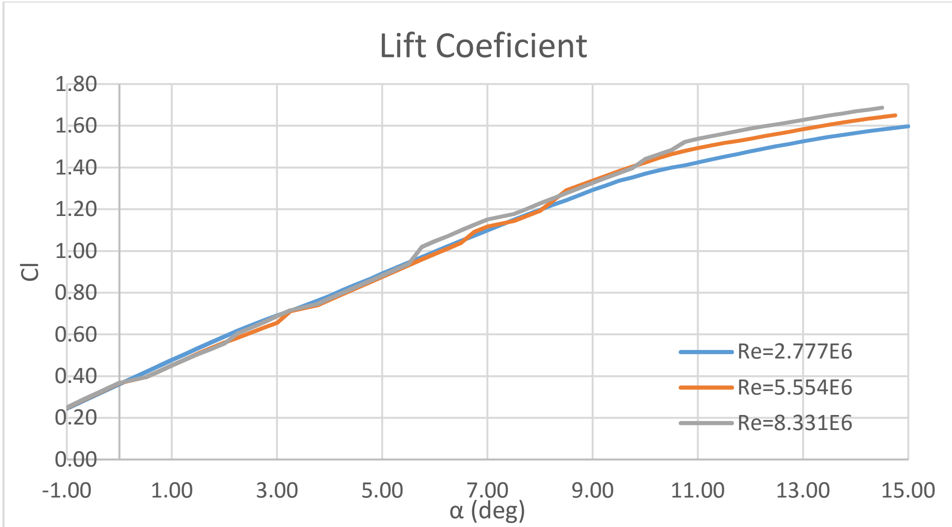
Lift Coeficient
Cl
α (deg)
Re=2.777E6
Re=5.554E6
Re=8.331E6

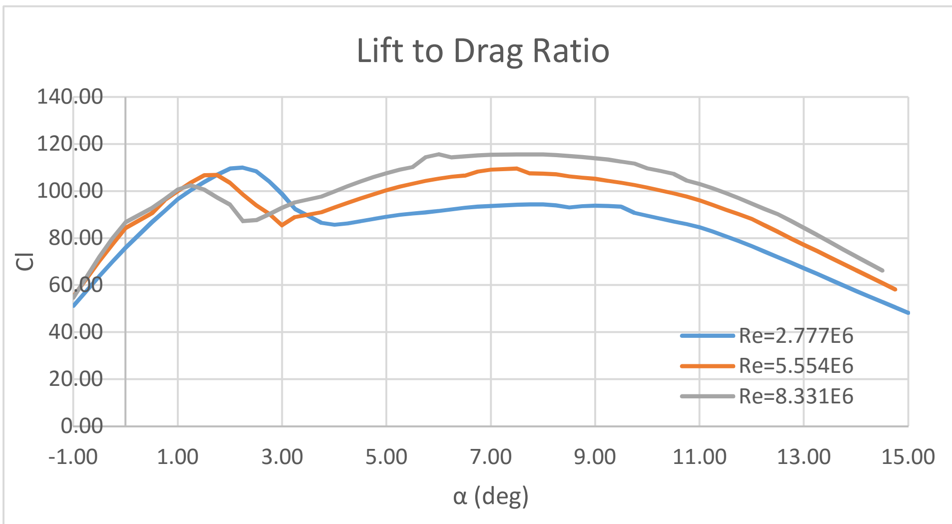
Lift to Drag Ratio
Cl
α (deg)
Re=2.777E6
Re=5.554E6
Re=8.331E6

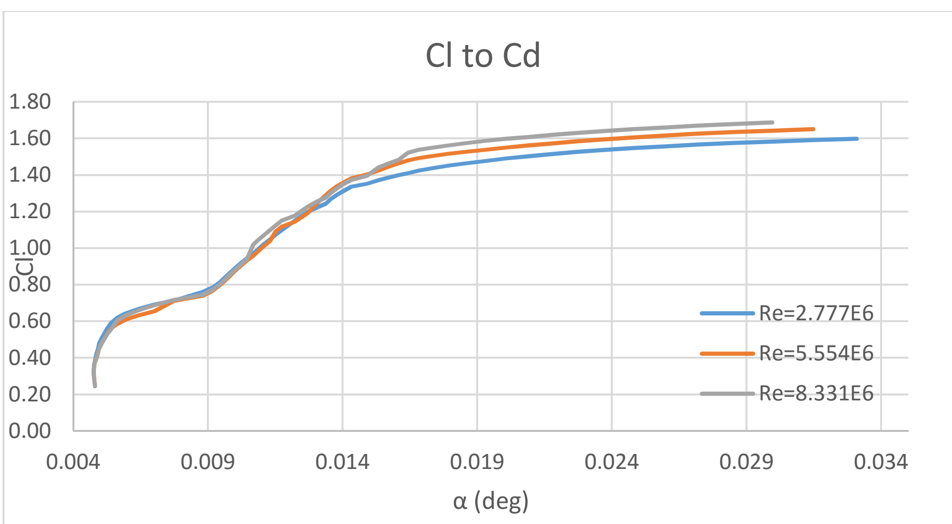
Cl to Cd
Cl
α (deg)
Re=2.777E6
Re=5.554E6
Re=8.331E6

APPENDIX B: STAR CCM+ SUMMARY REPORT

STAR CCM+ SUMMARY REPORT

The following table is a comprehensive list of the settings selected for this FSI simulation within STAR CCM+. These settings could be used to replicate the results of this thesis, or as a basis for a similar FSI study. These particular settings apply to free surface flow past a three-dimensional foil coupled with an isotropic structural analysis of the foil. These settings are selected within the simulation tree.

Summary Report: MM_1_a3_45kt

Session Summary	
Date	5/17/2016 21:27
Simulation	C:\Users\LAB\Desktop\Deformed\45kt\MM_1_a3_45kt.sim
File size	3.0e+03 MB
Number of Partitions	1
Number of Restored Partitions	15
Software Summary	
Version	BuildArch: win64 BuildEnv: intel15.0-r8 ReleaseDate: Tue Feb 2 20:59:21 UTC 2016 ReleaseNumber: 11.02.009
Hardware Summary	
Hosts	Number Processes: 1 Rank[0]: Couchlab_5.campus.webb-institute.edu

Simulation Properties

1 **MM_1_a3_45kt**		
+-1 Tags		
+-2 Contacts		
| `-1 Part Contact	Part 1	[Subtract]
| |	Part 2	[AC50 Foil noTE]
| +-1 In Place Contact	Part Surface 1	[Subtract.AC50 Foil noTE.Lower Bearing]

| |	Part Surface 2	[AC50 Foil noTE.Lower Bearing]
| |	Tags	[]
| |	Metadata	{}
| |	Index	1
| |	Interface	[Solid/Fluid]
| +-2 In Place Contact	Part Surface 1	[Subtract.AC50 Foil noTE.Tip]
| |	Part Surface 2	[AC50 Foil noTE.Tip]
| |	Tags	[]
| |	Metadata	{}
| |	Index	2
| |	Interface	[Solid/Fluid]
| +-3 In Place Contact	Part Surface 1	[Subtract.AC50 Foil noTE.Upper Bearing]
| |	Part Surface 2	[AC50 Foil noTE.Upper Bearing]
| |	Tags	[]
| |	Metadata	{}
| |	Index	3
| |	Interface	[Solid/Fluid]
| `-4 In Place Contact	Part Surface 1	[Subtract.AC50 Foil noTE.Upper Foil]
|	Part Surface 2	[AC50 Foil noTE.Upper Foil]
|	Tags	[]
|	Metadata	{}
|	Index	5
|	Interface	[Solid/Fluid]
+-3 3D-CAD Models		
+-4 Parts		
| +-1 **AC50 Foil noTE**	Tags	[]
| | |	Metadata	{}
| | |	Index	30
| | |	Region	[Solid]
| | |	Contacts	[Subtract]
| | |	Descriptions	[Root, FE Mesh.Remesh]
| | |	Face Count	5658
| | +-1 Surfaces		
| | | +-1 **Lower Bearing**	Tags	[]
| | | |	Metadata	{}
| | | |	Index	60

| | | |	Boundary	[Solid: Default]
| | | +-2 **Tip**	Tags	[]
| | | |	Metadata	{}
| | | |	Index	58
| | | |	Boundary	[Solid: Default]
| | | +-3 **Upper Bearing**	Tags	[]
| | | |	Metadata	{}
| | | |	Index	59
| | | |	Boundary	[Solid: Default]
| | | `-4 **Upper Foil**	Tags	[]
| | |	Metadata	{}
| | |	Index	62
| | |	Boundary	[Solid: Default]
| | `-2 Curves		
| | `-1 **Edges**	Tags	[]
| |	Feature Curve	[Solid:Default]
| |	Index	60
| +-2 **AC50 Hull**	Tags	[]
| | |	Metadata	{}
| | |	Index	27
| | |	Region	[]
| | |	Contacts	[]
| | |	Descriptions	[Root]
| | |	Face Count	7188
| | +-1 Surfaces		
| | | `-1 **Faces**	Tags	[]
| | |	Metadata	{}
| | |	Index	44
| | |	Boundary	[]
| | `-2 Curves		
| | `-1 **Edges**	Tags	[]
| |	Feature Curve	[]
| |	Index	47
| +-3 **Block Domain**	Tags	[]
| | |	Metadata	{}
| | |	Index	32
| | |	Region	[]
| | |	Contacts	[]

| | |	Descriptions	[Root]
| | |	Face Count	12
| | |	Coordinate System	Laboratory
| | |	Corner 1	[-8.0, -8.0, -4.126819605667171] m,m,m
| | |	Corner 2	[20.0, 8.0, 1.3894593180372503] m,m,m
| | +-1 Surfaces		
| | | +-1 **Inlet**	Tags	[]
| | | |	Metadata	{}
| | | |	Index	68
| | | |	Boundary	[]
| | | `-2 **Outlet**	Tags	[]
| | |	Metadata	{}
| | |	Index	69
| | |	Boundary	[]
| | `-2 Curves		
| | `-1 **Block Curve**	Tags	[]
| |	Feature Curve	[]
| |	Index	65
| +-4 **FS Ansi**	Tags	[]
| | |	Metadata	{}
| | |	Index	31
| | |	Region	[]
| | |	Contacts	[]
| | |	Descriptions	[Root]
| | |	Face Count	12
| | |	Coordinate System	Laboratory
| | |	Corner 1	[-0.07832586389971391, -0.14873311881873197, -0.12016268139345765] m,m,m
| | |	Corner 2	[0.8521969937304461, 0.17149382950573722, 0.23826276579279593] m,m,m
| | +-1 Surfaces		
| | | `-1 **Block Surface**	Tags	[]
| | |	Metadata	{}
| | |	Index	67
| | |	Boundary	[]

| | `-2 Curves		
| | `-1 **Block Curve**	Tags	[]
| |	Feature Curve	[]
| |	Index	64
| +-5 **FS Ref**	Tags	[]
| | |	Metadata	{}
| | |	Index	19
| | |	Region	[Fluid]
| | |	Contacts	[]
| | |	Descriptions	[Root]
| | |	Face Count	12
| | |	Coordinate System	Laboratory
| | |	Corner 1	[-11.507212389678276, -10.004121365530464, -0.075] m,m,m
| | |	Corner 2	[23.507212389678262, 10.004121365530464, 0.075] m,m,m
| | +-1 Surfaces		
| | | `-1 **Block Surface**	Tags	[]
| | |	Metadata	{}
| | |	Index	32
| | |	Boundary	[]
| | `-2 Curves		
| | `-1 **Block Curve**	Tags	[]
| |	Feature Curve	[Fluid:Default Feature Curve]
| |	Index	31
| +-6 **FS Wake**	Tags	[]
| | |	Metadata	{}
| | |	Index	33
| | |	Region	[]
| | |	Contacts	[]
| | |	Descriptions	[Root]
| | |	Face Count	12
| | |	Coordinate System	Laboratory
| | |	Corner 1	[6.857255144341117, -1.7643952882082048, -0.32805323169499445] m,m,m
| | |	Corner 2	[20.2986592585389, 2.0640645658530903, 0.17475387725446856] m,m,m

| | +-1 Surfaces		
| | | `-1 **Block Surface**	Tags	[]
| | |	Metadata	{}
| | |	Index	72
| | |	Boundary	[]
| | `-2 Curves		
| | `-1 **Block Curve**	Tags	[]
| |	Feature Curve	[]
| |	Index	68
| `-7 **Subtract**	Tags	[]
| |	Metadata	{}
| |	Index	13
| |	Region	[Fluid]
| |	Contacts	[AC50 Foil noTE]
| |	Descriptions	[Root, CFD Mesh.Remesh]
| |	Face Count	5670
| |	Operation	[Subtract]
+-5 Operations		
| +-1 **Subtract**	Perform CAD Boolean	FALSE
| | |	Input Parts	[AC50 Foil noTE, Block Domain]
| | |	Target Part	[Block Domain]
| | |	Output Parts	[Subtract]
| | `-1 Remesh Intersection Curve	Remesh Intersection Curve	FALSE
| +-2 **CFD Mesh**	Per-Part Meshing	FALSE
| | |	Mesher Execution Mode	Parallel
| | |	Input Parts	[Subtract]
| | |	Perform Local Surface Meshing	FALSE
| | |	Preserve Surface Perimeters	None
| | |	Verbose Output	FALSE
| | +-1 Meshers		
| | | +-1 Surface Remesher	Perform Curvature Refinement	TRUE
| | | |	Perform Proximity Refinement	TRUE
| | | |	Perform Compatibility Refinement	FALSE
| | | |	Create Aligned Meshes	TRUE
| | | |	Minimum Face Quality	0.05
| | | +-2 Trimmed Cell Mesher	Core Cell Type	Hexahedra

					Coordinate System	Laboratory
					Perform Mesh Alignment	FALSE
					Size Dependent Growth Rates	All cells
					Run Optimizer	TRUE
			`-3 Prism Layer Mesher	Stretching Function	Geometric Progression
				Distribution Mode	Stretch Factor
				Boundary March Angle	50
				Gap Fill Percentage	25
				Minimum Thickness Percentage	10
				Layer Reduction Percentage	50
				Concave Angle Limit	0
				Convex Angle Limit	360
				Near Core Layer Aspect Ratio	0
		+-2 Default Controls		
			+-1 Base Size	Value	0.05 m
			+-2 CAD Projection	Project to CAD	TRUE
			+-3 Target Surface Size	Size Type	Relative to base
				`-1 Relative Size	Percentage of Base	100
					Absolute Size	0.05 m
			+-4 Minimum Surface Size	Size Type	Relative to base
				`-1 Relative Size	Percentage of Base	0.001
					Absolute Size	5.0E-7 m
			+-5 Surface Curvature	Enable Curvature Deviation Distance	TRUE
				+-1 Basic Curvature	# Pts/circle	100
				`-2 Curvature Deviation	Max # Pts/circle	200
					Curvature Deviation Distance	1.0E-5 m
			+-6 Surface Proximity	Search Floor	0.0 m
					# Points in gap	2
					Enable Search Ceiling	FALSE
			+-7 Surface Growth Rate	Surface Growth Rate	1.3
			+-8 Number of Prism Layers	Number of Prism Layers	12
			+-9 Prism Layer Stretching	Prism Layer Stretching	1.6206

| | | +-10 Prism Layer Total Thickness	Size Type	Absolute
| | | | `-1 Absolute Size	Value	0.02 m
| | | +-11 Maximum Core/Prism Transition Ratio	Limit Cell Size by Prism Layer Thickness	FALSE
| | | +-12 Volume Growth Rate	Default Growth Rate	Medium
| | | |	Surface Growth Rate	Slow
| | | `-13 Maximum Cell Size	Size Type	Relative to base
| | | `-1 Relative Size	Percentage of Base	10000
| | |	Absolute Size	5.0 m
| | `-3 Custom Controls		
| | +-1 **1m Ref**	Enable Control	Enabled
| | | |	Controls Display Mode	All
| | | |	Part Surfaces	[Subtract.AC50 Foil noTE, Subtract.AC50 Foil noTE.Lower Bearing, Subtract.AC50 Foil noTE.Tip, Subtract.AC50 Foil noTE.Upper Bearing, Subtract.AC50 Foil noTE.Upper Foil]
| | | |	Apply Only to Contacting Area	Disabled
| | | +-1 Controls		
| | | | +-1 Target Surface Size	Target Surface Size	Parent
| | | | +-2 Minimum Surface Size	Minimum Surface Size	Parent
| | | | +-3 Surface Curvature	Curvature	Parent
| | | | +-4 Surface Proximity	Proximity	Parent
| | | | +-5 Edge Proximity	Proximity	Parent
| | | | +-6 Surface Growth Rate	Surface Growth Rate	Parent
| | | | +-7 Surface Remeshing	Surface Remeshing	Parent
| | | | +-8 Prism Layers	Prism Layers	Parent
| | | | +-9 Trimmer Surface Growth Rate	Trimmer Surface Growth Rate	Parent
| | | | +-10 Remesher Wake Refinement	Specify wake refinement options	Disabled
| | | | `-11 Trimmer Wake Refinement	Specify Trimmer Wake Refinement Options	Enabled

| | | `-2 Values		
| | | `-1 Wake Refinement	Size type	Relative to base
| | | |	Distance	1.0 m
| | | |	Direction	[1.0, 0.12, 0.0]
| | | |	Spread Angle	3.0 deg
| | | +-1 Relative Size	Percentage of Base	25
| | | |	Absolute Size	0.0125 m
| | | `-2 Trimmer Wake Refinement	Default Growth Rate	Medium
| | |	Surface Growth Rate	Disable
| | |	Customize Orthotropic Size	Disabled
| | +-2 **Foil**	Enable Control	Enabled
| | | |	Controls Display Mode	All
| | | |	Part Surfaces	[Subtract.AC50 Foil noTE.Lower Bearing, Subtract.AC50 Foil noTE.Upper Bearing, Subtract.AC50 Foil noTE.Upper Foil]
| | | |	Apply Only to Contacting Area	Disabled
| | | +-1 Controls		
| | | | +-1 Target Surface Size	Target Surface Size	Custom
| | | | +-2 Minimum Surface Size	Minimum Surface Size	Custom
| | | | +-3 Surface Curvature	Curvature	Custom
| | | | +-4 Surface Proximity	Proximity	Parent
| | | | +-5 Edge Proximity	Proximity	Custom
| | | | +-6 Surface Growth Rate	Surface Growth Rate	Parent
| | | | +-7 Surface Remeshing	Surface Remeshing	Parent
| | | | +-8 Prism Layers	Prism Layers	Parent
| | | | +-9 Trimmer Surface Growth Rate	Trimmer Surface Growth Rate	Parent
| | | | +-10 Remesher Wake Refinement	Specify wake refinement options	Disabled
| | | | `-11 Trimmer Wake Refinement	Specify Trimmer Wake Refinement Options	Enabled
| | | `-2 Values		
| | | +-1 Target Surface Size	Size Type	Relative to base

<table>
<tr><td>| | | | `-1 Relative Size</td><td>Percentage of Base</td><td>100</td></tr>
<tr><td>| | | |</td><td>Absolute Size</td><td>0.05 m</td></tr>
<tr><td>| | | +-2 Minimum Surface Size</td><td>Size Type</td><td>Relative to base</td></tr>
<tr><td>| | | | `-1 Relative Size</td><td>Percentage of Base</td><td>6.25</td></tr>
<tr><td>| | | |</td><td>Absolute Size</td><td>0.003125 m</td></tr>
<tr><td>| | | +-3 Surface Curvature</td><td>Enable Curvature Deviation Distance</td><td>TRUE</td></tr>
<tr><td>| | | | +-1 Basic Curvature</td><td># Pts/circle</td><td>100</td></tr>
<tr><td>| | | | `-2 Curvature Deviation</td><td>Max # Pts/circle</td><td>200</td></tr>
<tr><td>| | | |</td><td>Curvature Deviation Distance</td><td>0.001 m</td></tr>
<tr><td>| | | +-4 Edge Proximity</td><td>Number of Faces</td><td>4</td></tr>
<tr><td>| | | |</td><td>Enable Search Ceiling</td><td>FALSE</td></tr>
<tr><td>| | | |</td><td>Search Floor</td><td>0.0 m</td></tr>
<tr><td>| | | |</td><td>Include Feature Edges</td><td>FALSE</td></tr>
<tr><td>| | | |</td><td>Include Patch Perimeters</td><td>FALSE</td></tr>
<tr><td>| | | `-5 Wake Refinement</td><td>Size type</td><td>Relative to base</td></tr>
<tr><td>| | | |</td><td>Distance</td><td>6.0 m</td></tr>
<tr><td>| | | |</td><td>Direction</td><td>[1.0, 0.04, 0.0]</td></tr>
<tr><td>| | | |</td><td>Spread Angle</td><td>3.6 deg</td></tr>
<tr><td>| | | +-1 Relative Size</td><td>Percentage of Base</td><td>50</td></tr>
<tr><td>| | | |</td><td>Absolute Size</td><td>0.025 m</td></tr>
<tr><td>| | | `-2 Trimmer Wake Refinement</td><td>Default Growth Rate</td><td>Very Slow</td></tr>
<tr><td>| | |</td><td>Surface Growth Rate</td><td>Slow</td></tr>
<tr><td>| | |</td><td>Customize Orthotropic Size</td><td>Disabled</td></tr>
<tr><td>| | +-3 Foil Tip</td><td>Enable Control</td><td>Enabled</td></tr>
<tr><td>| | | |</td><td>Controls Display Mode</td><td>All</td></tr>
<tr><td>| | | |</td><td>Part Surfaces</td><td>[Subtract.AC50 Foil noTE.Tip]</td></tr>
<tr><td>| | | |</td><td>Apply Only to Contacting Area</td><td>Disabled</td></tr>
<tr><td>| | | +-1 Controls</td><td></td><td></td></tr>
<tr><td>| | | | +-1 Target Surface Size</td><td>Target Surface Size</td><td>Parent</td></tr>
<tr><td>| | | | +-2 Minimum Surface Size</td><td>Minimum Surface Size</td><td>Custom</td></tr>
<tr><td>| | | | +-3 Surface Curvature</td><td>Curvature</td><td>Custom</td></tr>
<tr><td>| | | | +-4 Surface Proximity</td><td>Proximity</td><td>Parent</td></tr>
</table>

| | | | +-5 Edge Proximity	Proximity	Parent
| | | | +-6 Surface Growth Rate	Surface Growth Rate	Custom
| | | | +-7 Surface Remeshing	Surface Remeshing	Parent
| | | | +-8 Prism Layers	Prism Layers	Parent
| | | | +-9 Trimmer Surface Growth Rate	Trimmer Surface Growth Rate	Parent
| | | | +-10 Remesher Wake Refinement	Specify wake refinement options	Disabled
| | | | `-11 Trimmer Wake Refinement	Specify Trimmer Wake Refinement Options	Enabled
| | | `-2 Values		
| | | +-1 Minimum Surface Size	Size Type	Relative to base
| | | | `-1 Relative Size	Percentage of Base	1
| | | |	Absolute Size	5.0E-4 m
| | | +-2 Surface Curvature	Enable Curvature Deviation Distance	TRUE
| | | | +-1 Basic Curvature	# Pts/circle	50
| | | | `-2 Curvature Deviation	Max # Pts/circle	200
| | | |	Curvature Deviation Distance	0.001 m
| | | +-3 Surface Growth Rate	Surface Growth Rate	1.3
| | | `-4 Wake Refinement	Size type	Relative to base
| | | |	Distance	6.0 m
| | | |	Direction	[1.0, 0.0, -0.1]
| | | |	Spread Angle	2.0 deg
| | | +-1 Relative Size	Percentage of Base	50
| | | |	Absolute Size	0.025 m
| | | `-2 Trimmer Wake Refinement	Default Growth Rate	Fast
| | |	Surface Growth Rate	Disable
| | |	Customize Orthotropic Size	Disabled
| | +-4 **FS Iso**	Enable Control	Enabled
| | | |	Controls Display Mode	All
| | | |	Parts	[FS Ansi]
| | | +-1 Controls		
| | | | +-1 Surface Remesher	Customize Size	Disabled

| | | | +-2 Prism Layer Mesher	Customize Number of Layers	Disabled
| | | | |	Customize Total Thickness	Disabled
| | | | |	Customize Stretching	Disabled
| | | | `-3 Trimmer	Customize Isotropic Size	Enabled
| | | |	Customize Orthotropic Size	Disabled
| | | `-2 Values		
| | | `-1 Custom Size	Size Type	Relative to base
| | | `-1 Relative Size	Percentage of Base	20
| | |	Absolute Size	0.01 m
| | +-5 **FS Ref**	Enable Control	Enabled
| | | |	Controls Display Mode	All
| | | |	Parts	[FS Ref]
| | | +-1 Controls		
| | | | +-1 Surface Remesher	Customize Size	Disabled
| | | | +-2 Prism Layer Mesher	Customize Number of Layers	Disabled
| | | | |	Customize Total Thickness	Disabled
| | | | |	Customize Stretching	Disabled
| | | | `-3 Trimmer	Customize Isotropic Size	Disabled
| | | |	Customize Orthotropic Size	Enabled
| | | `-2 Values		
| | | `-1 Trimmer Orthotropic Size	Relative/Absolute	Relative to base
| | | |	Custom X Size	Disabled
| | | |	Custom Y Size	Disabled
| | | |	Custom Z Size	Enabled
| | | `-1 Relative Z Size	Percentage of Base	50
| | |	Absolute Size	0.025 m
| | +-6 **Inlet**	Enable Control	Enabled
| | | |	Controls Display Mode	All
| | | |	Part Surfaces	[Subtract, Subtract.Block Domain.Inlet 2]
| | | |	Apply Only to Contacting Area	Disabled
| | | +-1 Controls		
| | | | +-1 Target Surface Size	Target Surface Size	Custom
| | | | +-2 Minimum Surface Size	Minimum Surface Size	Custom

| | | | +-3 Surface Curvature	Curvature	Custom
| | | | +-4 Surface Proximity	Proximity	Parent
| | | | +-5 Edge Proximity	Proximity	Parent
| | | | +-6 Surface Growth Rate	Surface Growth Rate	Custom
| | | | +-7 Surface Remeshing	Surface Remeshing	Parent
| | | | +-8 Prism Layers	Prism Layers	Parent
| | | | +-9 Trimmer Surface Growth Rate	Trimmer Surface Growth Rate	Custom
| | | | +-10 Remesher Wake Refinement	Specify wake refinement options	Disabled
| | | | `-11 Trimmer Wake Refinement	Specify Trimmer Wake Refinement Options	Disabled
| | | `-2 Values		
| | | +-1 Target Surface Size	Size Type	Relative to base
| | | | `-1 Relative Size	Percentage of Base	10000
| | | |	Absolute Size	5.0 m
| | | +-2 Minimum Surface Size	Size Type	Relative to base
| | | | `-1 Relative Size	Percentage of Base	400
| | | |	Absolute Size	0.2 m
| | | +-3 Surface Curvature	Enable Curvature Deviation Distance	TRUE
| | | | +-1 Basic Curvature	# Pts/circle	1
| | | | `-2 Curvature Deviation	Max # Pts/circle	90
| | | |	Curvature Deviation Distance	0.01 m
| | | +-4 Surface Growth Rate	Surface Growth Rate	1.3
| | | `-5 Trimmer Surface Growth Rate	Trimmer Surface Growth Rate	Fast
| | +-7 **Outlet**	Enable Control	Enabled
| | | |	Controls Display Mode	All
| | | |	Part Surfaces	[Subtract, Subtract.Block Domain.Outlet 2]
| | | |	Apply Only to Contacting Area	Disabled
| | | +-1 Controls		
| | | | +-1 Target Surface Size	Target Surface Size	Custom

| | | | +-2 Minimum Surface Size	Minimum Surface Size	Custom
| | | | +-3 Surface Curvature	Curvature	Custom
| | | | +-4 Surface Proximity	Proximity	Parent
| | | | +-5 Edge Proximity	Proximity	Parent
| | | | +-6 Surface Growth Rate	Surface Growth Rate	Custom
| | | | +-7 Surface Remeshing	Surface Remeshing	Parent
| | | | +-8 Prism Layers	Prism Layers	Parent
| | | | +-9 Trimmer Surface Growth Rate	Trimmer Surface Growth Rate	Custom
| | | | +-10 Remesher Wake Refinement	Specify wake refinement options	Disabled
| | | | `-11 Trimmer Wake Refinement	Specify Trimmer Wake Refinement Options	Disabled
| | | `-2 Values		
| | | +-1 Target Surface Size	Size Type	Relative to base
| | | | `-1 Relative Size	Percentage of Base	10000
| | | |	Absolute Size	5.0 m
| | | +-2 Minimum Surface Size	Size Type	Relative to base
| | | | `-1 Relative Size	Percentage of Base	400
| | | |	Absolute Size	0.2 m
| | | +-3 Surface Curvature	Enable Curvature Deviation Distance	FALSE
| | | | `-1 Basic Curvature	# Pts/circle	1
| | | +-4 Surface Growth Rate	Surface Growth Rate	1.3
| | | `-5 Trimmer Surface Growth Rate	Trimmer Surface Growth Rate	Fast
| | `-8 **Wake FS Ref**	Enable Control	Enabled
| | |	Controls Display Mode	All
| | |	Parts	[FS Wake]
| | +-1 Controls		
| | | +-1 Surface Remesher	Customize Size	Disabled
| | | +-2 Prism Layer Mesher	Customize Number of Layers	Disabled
| | | |	Customize Total Thickness	Disabled

|| ||	Customize Stretching	Disabled
|| | `-3 Trimmer	Customize Isotropic Size	Enabled
|| |	Customize Orthotropic Size	Disabled
|| `-2 Values		
|| `-1 Custom Size	Size Type	Relative to base
|| `-1 Relative Size	Percentage of Base	400
||	Absolute Size	0.2 m
| `-3 **FE Mesh**	Per-Part Meshing	FALSE
||	Mesher Execution Mode	Serial
||	Input Parts	[AC50 Foil noTE]
||	Perform Local Surface Meshing	FALSE
||	Preserve Surface Perimeters	None
||	Verbose Output	FALSE
| +-1 Meshers		
|| +-1 Surface Remesher	Perform Curvature Refinement	TRUE
|||	Perform Proximity Refinement	TRUE
|||	Perform Compatibility Refinement	FALSE
|||	Create Aligned Meshes	TRUE
|||	Minimum Face Quality	0.05
|| `-2 Tetrahedral Mesher	Enable Growth Rate	FALSE
||	Optimization Cycles	1
||	Quality Threshold	0.4
| +-2 Default Controls		
|| +-1 Base Size	Value	0.01 m
|| +-2 CAD Projection	Project to CAD	TRUE
|| +-3 Target Surface Size	Size Type	Relative to base
||| `-1 Relative Size	Percentage of Base	100
|||	Absolute Size	0.01 m
|| +-4 Minimum Surface Size	Size Type	Relative to base
||| `-1 Relative Size	Percentage of Base	10
|||	Absolute Size	0.001 m
|| +-5 Surface Curvature	Enable Curvature Deviation Distance	FALSE
||| `-1 Basic Curvature	# Pts/circle	36
|| +-6 Surface Proximity	Search Floor	0.0 m
|||	# Points in gap	2

| | |	Enable Search Ceiling	FALSE
| | +-7 Surface Growth Rate	Surface Growth Rate	1.3
| | `-8 Mesh Density	Density	1
| |	Growth Factor	1
| `-3 Custom Controls		
+-6 Descriptions	Number of Children	4
| +-1 Root	Described Parts	[Subtract, FS Ref, AC50 Hull, AC50 Foil noTE, FS Ansi, Block Domain, FS Wake]
| +-2 CFD Mesh.Remesh	Described Parts	[Subtract]
| |	Faces	140898
| |	Vertices	70453
| +-3 FE Mesh.Remesh	Described Parts	[AC50 Foil noTE]
| |	Faces	904782
| |	Vertices	452393
| `-4 Latest	Described Parts	[Subtract, FS Ref, AC50 Hull, AC50 Foil noTE, FS Ansi, Block Domain, FS Wake]
|	Faces	1052916
|	Vertices	526474
+-7 Continua	Continua	3
| +-1 **Parts Meshes**	Interpolation Option	Nearest neighbor
| |	Regions	[Fluid, Solid]
| |	Interfaces	[Solid/Fluid]
| +-2 **Physics 1**	Regions	[Fluid]
| | |	Interfaces	[Solid/Fluid]
| | +-1 Models		
| | | +-1 Cell Quality Remediation		
| | | +-2 Eulerian Multiphase		
| | | | +-1 Eulerian Phases		
| | | | | +-1 **Water**	Index	1
| | | | | | `-1 Models		
| | | | | | +-1 Constant Density		
| | | | | | +-2 Energy		
| | | | | | +-3 Liquid		
| | | | | | | `-1 **H2O**	Database Material	H2O (Water) [Standard/Liquids]

| | | | | | | `-1 Material Properties		
| | | | | | | +-1 Density	Method	Constant
| | | | | | | | `-1 Constant	Value	997.561 kg/m^3
| | | | | | | +-2 Dynamic Viscosity	Method	Constant
| | | | | | | | `-1 Constant	Value	8.8871E-4 Pa-s
| | | | | | | +-3 Specific Heat	Method	Constant
| | | | | | | | `-1 Constant	Value	4181.72 J/kg-K
| | | | | | | `-4 Thermal Conductivity	Method	Constant
| | | | | | | `-1 Constant	Value	0.620271 W/m-K
| | | | | | `-4 Turbulent		
| | | | | `-2 **Air**	Index	2
| | | | | `-1 Models		
| | | | | +-1 Constant Density		
| | | | | +-2 Energy		
| | | | | +-3 Gas		
| | | | | | `-1 **Air**	Database Material	Air (Air) [Standard/Gases]
| | | | | | `-1 Material Properties		
| | | | | | +-1 Density	Method	Constant
| | | | | | | `-1 Constant	Value	1.18415 kg/m^3
| | | | | | +-2 Dynamic Viscosity	Method	Constant
| | | | | | | `-1 Constant	Value	1.85508E-5 Pa-s
| | | | | | +-3 Specific Heat	Method	Constant
| | | | | | | `-1 Constant	Value	1003.62 J/kg-K
| | | | | | `-4 Thermal Conductivity	Method	Constant
| | | | | | `-1 Constant	Value	0.0260305 W/m-K
| | | | | `-4 Turbulent		
| | | | `-2 **Mixture**		
| | | | `-1 Material Properties		
| | | | +-1 Dynamic Viscosity	Method	Volume-Weighted Mixture
| | | | | `-1 Volume-Weighted Mixture		
| | | | +-2 Specific Heat	Method	Mass-Weighted Mixture

| | | | | `-1 Mass-Weighted Mixture		
| | | | +-3 Thermal Conductivity	Method	Volume-Weighted Mixture
| | | | | `-1 Volume-Weighted Mixture		
| | | | `-4 Turbulent Prandtl Number	Method	Constant
| | | | `-1 Constant	Value	0.9
| | | +-3 Exact Wall Distance		
| | | +-4 Gradients	Gradient Method	Hybrid Gauss-LSQ
| | | |	Limiter Method	Venkatakrishnan
| | | |	Custom Accuracy Level Selector	2
| | | |	Verbose	FALSE
| | | |	Least-Squares Quality Criterion	TRUE
| | | |	Flat Cells Curvature Criterion	TRUE
| | | |	Cell Skewness Criterion	TRUE
| | | |	Chevron-Cell Criterion	TRUE
| | | |	Least-Squares Tensor Minimum Eigenvalues Ratio	0.1
| | | |	Normalized Flat Cells Curvature Factor	1
| | | |	Maximum Safe (Positive) Skewness Angle (deg)	75
| | | |	Minimum Unsafe (Positive) Skewness Angle (deg)	88
| | | |	Use TVB Gradient Limiting	FALSE
| | | |	Acceptable Field Variation (Factor)	0.05
| | | +-5 Gravity		
| | | +-6 K-Epsilon Turbulence		
| | | +-7 Multiphase Equation of State		
| | | +-8 Multiphase Interaction		
| | | | `-1 Phase Interactions		
| | | +-9 Realizable K-Epsilon Two-Layer	Buoyancy Production of Dissipation	Boundary Layer Orientation
| | | |	Cmu	0.09
| | | |	C1e	1.44
| | | |	C2e	1.9
| | | |	Ct	1

| | | |	Sigma_k	1
| | | |	Sigma_e	1.2
| | | |	Sarkar	2
| | | |	Tke Minimum	1.00E-10
| | | |	Tdr Minimum	1.00E-10
| | | |	Secondary Gradients	On
| | | |	Convection	2nd-order
| | | |	Normal Stress Term	FALSE
| | | |	Curvature Correction Option	Off
| | | |	Two-Layer Type	Shear Driven (Wolfstein)
| | | |	Two-Layer ReY*	60
| | | |	Two-Layer Delta ReY	10
| | | +-10 Reynolds-Averaged Navier-Stokes		
| | | +-11 Segregated Flow	Minimum Absolute Pressure	1000.0 Pa
| | | |	Flow Boundary Diffusion	TRUE
| | | |	Unsteady Flux Dissipation Corrections	FALSE
| | | |	Limit Acoustic-CFL Option	Per-Model
| | | |	Secondary Gradients	On
| | | |	Convection	2nd-order
| | | |	Delta-V Dissipation	Off
| | | +-12 Segregated Multiphase Temperature	Secondary Gradients	On
| | | |	Convection	2nd-order
| | | |	Flow Boundary Diffusion	TRUE
| | | +-13 Steady		
| | | +-14 Three Dimensional		
| | | +-15 Turbulent		
| | | +-16 Two-Layer All y+ Wall Treatment	Iterative Ustar	FALSE
| | | +-17 VOF Waves	Damping Constant 1	10
| | | | |	Damping Constant 2	10
| | | | |	Damping Exponent	2
| | | | |	Enable Theory Comparison	FALSE
| | | | `-1 Waves		
| | | | `-1 **FlatVofWave 1**	Point On Water Level	[0.0, 0.0, 0.0] m
| | | |	Vertical Direction	[0.0, 0.0, 1.0]
| | | |	Current	[20.0, 0.0, 0.0] m/s

| | | |	Wind	[20.0, 0.0, 0.0] m/s
| | | |	Light Fluid Density	1.18415 kg/m^3
| | | |	Heavy Fluid Density	1025.0 kg/m^3
| | | `-18 Volume of Fluid (VOF)	Convection	2nd-order
| | |	Compressibility Enhancement	FALSE
| | |	Sharpening Factor	0
| | |	Angle Factor	0.05
| | |	CFL_l	50
| | |	CFL_u	100
| | +-2 Reference Values		
| | | +-1 Gravity	Value	[0.0, 0.0, -9.81] m/s^2
| | | +-2 Reference Altitude	Value	[0.0, 0.0, 0.0] m
| | | +-3 Reference Density	Value	1.0 kg/m^3
| | | +-4 Minimum Allowable Wall Distance	Value	1.0E-6 m
| | | +-5 Minimum Allowable Temperature	Value	100.0 K
| | | +-6 Maximum Allowable Temperature	Value	5000.0 K
| | | `-7 Reference Pressure	Value	101325.0 Pa
| | `-3 Initial Conditions		
| | +-1 Pressure	Method	Field Function
| | | `-1 Field Function	Scalar Function	Hydrostatic Pressure of FlatVofWave 1
| | +-2 Static Temperature	Method	Constant
| | | `-1 Constant	Value	300.0 K
| | +-3 Turbulence Intensity	Method	Constant
| | | `-1 Constant	Value	0.01
| | +-4 Turbulence Specification	Method	Intensity + Viscosity Ratio
| | +-5 Turbulent Velocity Scale	Method	Constant
| | | `-1 Constant	Value	1.0 m/s
| | +-6 Turbulent Viscosity Ratio	Method	Constant
| | | `-1 Constant	Value	10
| | +-7 Velocity	Method	Field Function

| | | |	Coordinate System	Laboratory
| | | `-1 Field Function	Vector Function	Velocity of FlatVofWave 1
| | `-8 Volume Fraction	Method	Composite
| | `-1 Composite		
| | +-1 ScalarProfile	Method	Field Function
| | | `-1 Field Function	Scalar Function	Volume Fraction of Heavy Fluid of FlatVofWave 1
| | `-2 ScalarProfile	Method	Field Function
| | `-1 Field Function	Scalar Function	Volume Fraction of Light Fluid of FlatVofWave 1
| `-3 **Solid Physics**	Regions	[Solid]
| |	Interfaces	[Solid/Fluid]
| +-1 Models		
| | +-1 Cell Quality Remediation		
| | +-2 Fluid Structure Coupling		
| | +-3 Gravity		
| | +-4 Linear Isotropic Elastic		
| | +-5 Solid		
| | | `-1 **Al**	Database Material	Al (Aluminum (pure)) [Standard/Solids]
| | | `-1 Material Properties		
| | | +-1 Density	Method	Constant
| | | | `-1 Constant	Value	2702.0 kg/m^3
| | | +-2 Poisson's Ratio	Method	Constant
| | | | `-1 Constant	Value	0.33
| | | `-3 Young's Modulus	Method	Constant
| | | `-1 Constant	Value	68000.0 MPa
| | +-6 Solid Stress	Nonlinear Geometry	FALSE
| | +-7 Steady		
| | `-8 Three Dimensional		
| +-2 Reference Values		
| | `-1 Gravity	Value	[0.0, 0.0, -9.81] m/s^2
| `-3 Initial Conditions		
| `-1 Displacement	Method	Constant
| |	Coordinate System	Laboratory
| `-1 Constant	Value	[0.0, 0.0, 0.0] m

+-8 Regions	Regions	2
| +-1 **Fluid**	Index	1
| | |	Mesh Continuum	Parts Meshes
| | |	Physics Continuum	Physics 1
| | |	Parts	[Subtract, FS Ref]
| | |	Type	Fluid Region
| | |	Allow Per-Part Values	FALSE
| | +-1 Boundaries	Boundaries	4
| | | +-1 **Flow Domain.Inlet**	Index	18
| | | | |	Interfaces	
| | | | |	Part Surfaces	[Subtract.Block Domain.Inlet 2]
| | | | |	Type	Velocity Inlet
| | | | |	Allow Per-Surface Values	FALSE
| | | | +-1 Physics Conditions		
| | | | | +-1 Morpher	Method	Fixed
| | | | | +-2 Reference Frame Specification	Option	Lab Frame
| | | | | +-3 Turbulence Specification	Method	Intensity + Viscosity Ratio
| | | | | `-4 Velocity Specification	Method	Components
| | | | `-2 Physics Values		
| | | | +-1 Morpher: Thin Factor	Vertex Thin Factor	1
| | | | +-2 Static Temperature	Method	Constant
| | | | | `-1 Constant	Value	300.0 K
| | | | +-3 Turbulence Intensity	Method	Constant
| | | | | `-1 Constant	Value	0.01
| | | | +-4 Turbulent Viscosity Ratio	Method	Constant
| | | | | `-1 Constant	Value	10
| | | | +-5 Velocity	Method	Field Function
| | | | | |	Coordinate System	Laboratory
| | | | | `-1 Field Function	Vector Function	Velocity of FlatVofWave 1
| | | | `-6 Volume Fraction	Method	Composite
| | | | `-1 Composite		

| | | | +-1 ScalarProfile	Method	Field Function
| | | | | `-1 Field Function	Scalar Function	Volume Fraction of Heavy Fluid of FlatVofWave 1
| | | | `-2 ScalarProfile	Method	Field Function
| | | | `-1 Field Function	Scalar Function	Volume Fraction of Light Fluid of FlatVofWave 1
| | | +-2 **Flow Domain.Outlet**	Index	17
| | | | |	Interfaces	
| | | | |	Part Surfaces	[Subtract.Block Domain.Outlet 2]
| | | | |	Type	Pressure Outlet
| | | | |	Allow Per-Surface Values	TRUE
| | | | +-1 Physics Conditions		
| | | | | +-1 Backflow Specification	Direction	Boundary-Normal
| | | | | |	Pressure	Environmental
| | | | | +-2 Morpher	Method	Fixed
| | | | | +-3 Pressure Outlet Option	Option	None
| | | | | +-4 Reference Frame Specification	Option	Lab Frame
| | | | | `-5 Turbulence Specification	Method	Intensity + Viscosity Ratio
| | | | +-2 Physics Values		
| | | | | +-1 Morpher: Thin Factor	Vertex Thin Factor	1
| | | | | +-2 Pressure	Method	Field Function
| | | | | | `-1 Field Function	Scalar Function	Hydrostatic Pressure of FlatVofWave 1
| | | | | +-3 Static Temperature	Method	Constant
| | | | | | `-1 Constant	Value	300.0 K
| | | | | +-4 Turbulence Intensity	Method	Constant
| | | | | | `-1 Constant	Value	0.01
| | | | | +-5 Turbulent Viscosity Ratio	Method	Constant
| | | | | | `-1 Constant	Value	10
| | | | | `-6 Volume Fraction	Method	Composite
| | | | | `-1 Composite		
| | | | | +-1 ScalarProfile	Method	Field Function

| | | | | | `-1 Field Function	Scalar Function	Volume Fraction of Heavy Fluid of FlatVofWave 1
| | | | | `-2 ScalarProfile	Method	Field Function
| | | | | `-1 Field Function	Scalar Function	Volume Fraction of Light Fluid of FlatVofWave 1
| | | | `-3 Surface Subgroupings		
| | | | `-1 Subgrouping 1	Default Subgroup	[Subgroup 1]
| | | | `-1 Subgroup 1	Objects	[Subtract.Block Domain.Outlet 2]
| | | | `-1 **Block Domain.Outlet 2**	Tags	[]
| | | |	Metadata	{}
| | | |	Index	71
| | | |	Boundary	[Fluid: Flow Domain.Outlet]
| | | +-3 **Foil**	Index	19
| | | | |	Interfaces	
| | | | |	Part Surfaces	[Subtract.AC50 Foil noTE.Lower Bearing, Subtract.AC50 Foil noTE.Tip, Subtract.AC50 Foil noTE.Upper Bearing, Subtract.AC50 Foil noTE.Upper Foil]
| | | | |	Type	Wall
| | | | |	Allow Per-Surface Values	FALSE
| | | | +-1 Physics Conditions		
| | | | | +-1 Morpher	Method	Floating
| | | | | +-2 Reference Frame Specification	Option	Region Reference Frame
| | | | | +-3 Shear Stress Specification	Method	No-Slip
| | | | | +-4 Tangential Velocity Specification	Method	Fixed
| | | | | +-5 Thermal Specification	Condition	Adiabatic

| | | | | +-6 User Wall Heat Flux Coefficient Specification	Method	None
| | | | | `-7 Wall Surface Specification	Method	Smooth
| | | | `-2 Physics Values		
| | | | `-1 Blended Wall Function	E	9
| | | |	Kappa	0.42
| | | `-4 **Solid/Fluid [1]**	Index	46
| | | |	Interfaces	
| | | |	Part Surfaces	[]
| | | |	Type	Mapped Contact Boundary
| | | |	Allow Per-Contact Values	FALSE
| | | |	Parent Interface	Solid/Fluid
| | | +-1 Physics Conditions		
| | | | +-1 Morpher	Method	Solid Stress
| | | | +-2 Reference Frame Specification	Option	Region Reference Frame
| | | | +-3 Shear Stress Specification	Method	No-Slip
| | | | +-4 Tangential Velocity Specification	Method	Fixed
| | | | +-5 Thermal Specification	Condition	Adiabatic
| | | | +-6 User Wall Heat Flux Coefficient Specification	Method	None
| | | | `-7 Wall Surface Specification	Method	Smooth
| | | `-2 Physics Values		
| | | +-1 Blended Wall Function	E	9
| | | |	Kappa	0.42
| | | `-2 Morpher: Thin Factor	Vertex Thin Factor	1

| | +-2 Feature Curves	Feature Curves	1
| | | `-1 **Default Feature Curve**	Part Curves	[FS Ref.Block Curve, Subtract.AC50 Foil noTE.Edges, Subtract.Block Domain.Block Curve 2]
| | +-3 Physics Conditions		
| | | +-1 Energy Source Option	Energy Source Option	None
| | | +-2 Initial Condition Option	Option	Use Continuum Values
| | | +-3 Momentum Source Option	Momentum Source Option	None
| | | +-4 Phase Source Option	Phase Source Term	Disabled
| | | +-5 Turbulence Source Option	Turbulence Source Option	None
| | | `-6 VofWave Damping Option	VofWave Damping Option	No Damping
| | `-4 Physics Values		
| | +-1 Axis	Coordinate System	Laboratory
| | |	Origin	[0.0, 0.0, 0.0] m
| | |	Direction	[0.0, 0.0, 1.0]
| | +-2 Control Point List	Table: Control Point X0	null
| | |	Table: Control Point Y0	null
| | |	Table: Control Point Z0	null
| | |	Table: Control Point X1	null
| | |	Table: Control Point Y1	null
| | |	Table: Control Point Z1	null
| | `-3 Motion Specification	Motion	Morphing
| |	Reference Frame	Lab Reference Frame
| `-2 **Solid**	Index	2
| |	Mesh Continuum	Parts Meshes
| |	Physics Continuum	Solid Physics
| |	Parts	[AC50 Foil noTE]
| |	Type	Solid Region

| |	Allow Per-Part Values	FALSE
| +-1 Boundaries	Boundaries	2
| | +-1 **Default**	Index	20
| | | |	Interfaces	
| | | |	Part Surfaces	[AC50 Foil noTE.Tip, AC50 Foil noTE.Upper Bearing, AC50 Foil noTE.Lower Bearing, AC50 Foil noTE.Upper Foil]
| | | |	Type	Wall
| | | |	Allow Per-Surface Values	FALSE
| | | `-1 Physics Conditions		
| | | `-1 Stress/Displacement	Method	Free
| | `-2 **Solid/Fluid [0]**	Index	45
| |	Interfaces	
| |	Part Surfaces	[]
| |	Type	Mapped Contact Boundary
| |	Allow Per-Contact Values	FALSE
| |	Parent Interface	Solid/Fluid
| +-2 Feature Curves	Feature Curves	1
| | `-1 **Default**	Part Curves	[AC50 Foil noTE.Edges]
| +-3 Physics Conditions		
| | +-1 Body Load Option	Method	None
| | +-2 Initial Condition Option	Option	Use Continuum Values
| | `-3 Mid-side Vertex Option	Mid-side Vertex	Keep Original
| +-4 Physics Values		
| | +-1 Axis	Coordinate System	Laboratory
| | |	Origin	[0.0, 0.0, 0.0] m
| | |	Direction	[0.0, 0.0, 1.0]

| | `-2 Motion Specification	Motion	Solid Displacement
| |	Reference Frame	Lab Reference Frame
| `-5 Segments	Segments	3
| +-1 **Constraints**	Index	1
| | |	Surfaces	[AC50 Foil noTE.Lower Bearing[rem], AC50 Foil noTE.Lower Bearing[AC50 Foil noTE.Lower Bearing/Lower Bearing], AC50 Foil noTE.Upper Bearing[rem], AC50 Foil noTE.Upper Bearing[AC50 Foil noTE.Upper Bearing/Upper Bearing]]
| | |	Type	Constraint
| | `-1 Physics Conditions		
| | `-1 Solid Stress Constraints	Method	Fixed
| +-2 **Pressure**	Index	2
| | |	Surfaces	[]
| | |	Type	Load
| | +-1 Physics Conditions		
| | | +-1 Solid Stress Loads	Method	Pressure
| | | `-2 Surface Load Treatment Option	Method	Discontinuous
| | `-2 Physics Values		
| | `-1 Pressure	Method	Field Function
| | `-1 Field Function	Scalar Function	Pressure
| `-3 **Traction**	Index	3
| |	Surfaces	[]
| |	Type	Load
| +-1 Physics Conditions		

| | +-1 Solid Stress Loads	Method	Traction
| | `-2 Surface Load Treatment Option	Method	Discontinuous
| `-2 Physics Values		
| `-1 Traction	Method	Field Function
| |	Coordinate System	Laboratory
| `-1 Field Function	Vector Function	MappedVertexWallShearStress
+-9 Interfaces	Verbosity	FALSE
| |	Interfaces	1
| `-1 **Solid/Fluid**	Allow Per-Contact Values	FALSE
| |	Geometry	Contacts
| |	Contacts	[AC50 Foil noTE.Lower Bearing/Lower Bearing, AC50 Foil noTE.Tip/Tip, AC50 Foil noTE.Upper Bearing/Upper Bearing, AC50 Foil noTE.Upper Foil/Upper Foil]
| |	Type	Mapped Contact Interface
| |	Topology	Indirect
| |	Connectivity	Mapped
| `-1 Physics Values		
| `-1 Mapped Interface Tolerance	Proximity Check	TRUE
|	Minimum Proximity	0.05
|	Normal Directions Check	TRUE
|	Minimum Angle	110
|	Use Bounding Box Filtering	FALSE
+-10 Co-Simulations		
+-11 Derived Parts	Derived Parts	5
| +-1 **FS**	Parts	[Fluid, Fluid: Flow Domain.Inlet, Fluid: Flow Domain.Outlet, Fluid: Foil]
| | |	Scalar Field	Volume Fraction of Water
| | |	Mode	Single

| | `-1 Value	Isovalue	0.5
| +-2 **Isosurface**	Parts	[Fluid]
| | |	Scalar Field	Absolute Pressure
| | |	Mode	Multiple (range)
| | `-1 Values (Range)	Number of Isosurfaces	2
| |	Isovalue Range	[-513374.723, 3176.0] Pa
| +-3 **Plane Section**	Origin	[0.25, 0.0, 0.0] m,m,m
| | |	Coordinate System	Laboratory
| | |	Normal	[1.0, 0.0, 0.0] m,m,m
| | |	Parts	[Fluid]
| | |	Section Mode	Single Section
| | |	Displayed Index	-1
| | `-1 Single section	Offset	0.0 m
| +-4 **Plane Section 2**	Origin	[0.0, -2.15, 0.0] m,m,m
| | |	Coordinate System	Laboratory
| | |	Normal	[0.0, 1.0, 0.0] m,m,m
| | |	Parts	[Fluid]
| | |	Section Mode	Single Section
| | |	Displayed Index	-1
| | `-1 Single section	Offset	0.0 m
| `-5 **Vector Warp**	Parts	[Solid: Solid/Fluid [0]]
|	Vector Field	Displacement
|	Relative or Absolute Coordinates	Relative
|	Scale Factor	1
|	Auto-scaling	TRUE
+-12 Solvers		
| +-1 FE Stress	Env Variables	
| | |	Solver Frozen	FALSE
| | |	Verbosity	None
| | |	Temporary Storage Retained	FALSE
| | `-1 Sparse Direct Solver	Ordering	Serial
| |	Verbosity	None
| |	Mode	Auto

| |	Temp Write Directory	.
| |	Total Mem Allowed (MB)	196530
| |	Stop If Not Enough Mem	FALSE
| |	Number of Threads	1
| +-2 Fluid Structure Interaction	Solver Frozen	FALSE
| |	Verbosity	None
| |	Temporary Storage Retained	FALSE
| |	Method	Two Way
| +-3 Mesh Morpher	Automatic Thinner Version	0
| |	Solver Frozen	FALSE
| |	Verbosity	None
| |	Morph From Zero	FALSE
| |	Morpher Tolerance	1.00E-07
| |	Initialization Needs Morphing	FALSE
| |	Recompute Interfaces	TRUE
| |	Skip Thinned Vertex Corrector	FALSE
| |	Temporary Storage Retained	FALSE
| +-4 Partitioning	Solver Frozen	FALSE
| |	Partitioning Method	Per-Continuum
| +-5 Wall Distance	Solver Frozen	FALSE
| |	Verbosity	0
| |	Minimum Tree Size Threshold	500000
| |	Use SFC/SIMD	FALSE
| +-6 Damping Boundary Distance	Solver Frozen	FALSE
| |	Verbosity	0
| |	Minimum Tree Size Threshold	500000
| +-7 Segregated Flow	Freeze Flow	FALSE
| | |	Reconstruction Frozen	FALSE
| | |	Reconstruction Zeroed	FALSE
| | |	Enable Enhanced Stability Treatment	FALSE
| | |	Temporary Storage Retained	FALSE
| | |	Pressure Corrections: Bad Cell Minimum Scaling	0.8

<table>
<tr><td>| | |</td><td>Pressure Corrections: Acceptable Cell Volume Change</td><td>0.001</td></tr>
<tr><td>| | |</td><td>Velocity Corrections: Maximum Unlimited Velocity</td><td>20.0 m/s</td></tr>
<tr><td>| | |</td><td>Velocity Corrections: Acceptable Velocity Increase Rate [<1]</td><td>0.15</td></tr>
<tr><td>| | |</td><td>Continuity Initialization</td><td>FALSE</td></tr>
<tr><td>| | +-1 Velocity</td><td>Under-Relaxation Factor</td><td>0.7</td></tr>
<tr><td>| | | |</td><td>Dynamic Local Under-Relaxation</td><td>FALSE</td></tr>
<tr><td>| | | +-1 Under-Relaxation Factor Ramp</td><td>Ramp Method</td><td>No Ramp</td></tr>
<tr><td>| | | `-2 AMG Linear Solver</td><td>Max Cycles</td><td>30</td></tr>
<tr><td>| | | |</td><td>Verbosity</td><td>None</td></tr>
<tr><td>| | | |</td><td>Enable Direct Solver</td><td>FALSE</td></tr>
<tr><td>| | | |</td><td>Maximum Direct Solver Equations</td><td>32</td></tr>
<tr><td>| | | |</td><td>Convergence Tolerance</td><td>0.1</td></tr>
<tr><td>| | | |</td><td>Epsilon</td><td>0</td></tr>
<tr><td>| | | |</td><td>Cycle Type</td><td>Flex Cycle</td></tr>
<tr><td>| | | |</td><td>Group Size Control</td><td>Auto</td></tr>
<tr><td>| | | |</td><td>Group Size</td><td>4</td></tr>
<tr><td>| | | |</td><td>Relaxation Scheme</td><td>Gauss-Seidel</td></tr>
<tr><td>| | | |</td><td>Acceleration Method</td><td>None</td></tr>
<tr><td>| | | |</td><td>Scaling</td><td>Disabled</td></tr>
<tr><td>| | | `-1 Flex Cycle</td><td>Restriction Tolerance</td><td>0.9</td></tr>
<tr><td>| | |</td><td>Prolongation Tolerance</td><td>0.5</td></tr>
<tr><td>| | |</td><td>Sweeps</td><td>1</td></tr>
<tr><td>| | `-2 Pressure</td><td>Number of Non-Orthogonality Correctors</td><td>0</td></tr>
<tr><td>| | |</td><td>Under-Relaxation Factor</td><td>0.3</td></tr>
<tr><td>| | |</td><td>Pressure Reference Location</td><td>Automatic Selection</td></tr>
<tr><td>| | +-1 Under-Relaxation Factor Ramp</td><td>Ramp Method</td><td>No Ramp</td></tr>
<tr><td>| | `-2 AMG Linear Solver</td><td>Max Cycles</td><td>30</td></tr>
<tr><td>| | |</td><td>Verbosity</td><td>None</td></tr>
<tr><td>| | |</td><td>Enable Direct Solver</td><td>FALSE</td></tr>
</table>

| | |	Maximum Direct Solver Equations	32
| | |	Convergence Tolerance	0.1
| | |	Epsilon	0
| | |	Cycle Type	V Cycle
| | |	Group Size Control	Auto
| | |	Group Size	4
| | |	Relaxation Scheme	Gauss-Seidel
| | |	Acceleration Method	Conjugate Gradient
| | |	Scaling	Auto
| | `-1 V Cycle	Pre-Sweeps	1
| |	Post-Sweeps	1
| |	Max Levels	50
| +-8 Segregated VOF	Solver Frozen	FALSE
| | |	Reconstruction Frozen	FALSE
| | |	Reconstruction Zeroed	FALSE
| | |	Temporary Storage Retained	FALSE
| | |	Under-Relaxation Factor	0.9
| | +-1 Under-Relaxation Factor Ramp	Ramp Method	No Ramp
| | `-2 AMG Linear Solver	Max Cycles	30
| | |	Verbosity	None
| | |	Enable Direct Solver	FALSE
| | |	Maximum Direct Solver Equations	32
| | |	Convergence Tolerance	0.1
| | |	Epsilon	0
| | |	Cycle Type	V Cycle
| | |	Group Size Control	Auto
| | |	Group Size	4
| | |	Relaxation Scheme	Gauss-Seidel
| | |	Acceleration Method	None
| | |	Scaling	Disabled
| | `-1 V Cycle	Pre-Sweeps	1
| |	Post-Sweeps	1

| |	Max Levels	50
| +-9 Segregated Energy	Solver Frozen	FALSE
| | |	Reconstruction Frozen	FALSE
| | |	Reconstruction Zeroed	FALSE
| | |	Temporary Storage Retained	FALSE
| | |	Fluid Under-Relaxation Factor	0.9
| | |	Solid Under-Relaxation Factor	0.99
| | +-1 Fluid Under-Relaxation Factor Ramp	Ramp Method	No Ramp
| | +-2 Solid Under-Relaxation Factor Ramp	Ramp Method	No Ramp
| | `-3 AMG Linear Solver	Max Cycles	30
| | |	Verbosity	None
| | |	Enable Direct Solver	FALSE
| | |	Maximum Direct Solver Equations	32
| | |	Convergence Tolerance	0.1
| | |	Epsilon	0
| | |	Cycle Type	V Cycle
| | |	Group Size Control	Auto
| | |	Group Size	4
| | |	Relaxation Scheme	Gauss-Seidel
| | |	Acceleration Method	None
| | |	Scaling	Disabled
| | `-1 V Cycle	Pre-Sweeps	1
| |	Post-Sweeps	1
| |	Max Levels	50
| +-10 K-Epsilon Turbulence	Solver Frozen	FALSE
| | |	Reconstruction Frozen	FALSE
| | |	Reconstruction Zeroed	FALSE
| | |	Temporary Storage Retained	FALSE
| | |	Under-Relaxation Factor	0.8
| | |	Boundary Layer Initialization	FALSE

| | +-1 Under-Relaxation Factor Ramp	Ramp Method	No Ramp
| | `-2 AMG Linear Solver	Max Cycles	30
| | |	Verbosity	None
| | |	Enable Direct Solver	FALSE
| | |	Maximum Direct Solver Equations	32
| | |	Convergence Tolerance	0.1
| | |	Epsilon	0
| | |	Cycle Type	Flex Cycle
| | |	Group Size Control	Auto
| | |	Group Size	4
| | |	Relaxation Scheme	Gauss-Seidel
| | |	Acceleration Method	None
| | |	Scaling	Disabled
| | `-1 Flex Cycle	Restriction Tolerance	0.9
| |	Prolongation Tolerance	0.5
| |	Sweeps	1
| `-11 K-Epsilon Turbulent Viscosity	Solver Frozen	FALSE
|	Under-Relaxation Factor	1
|	Maximum Ratio	100000
+-13 Stopping Criteria		
| +-1 **Displacement Criterion**	Enabled	TRUE
| | |	Criterion Option	Minimum
| | |	Logical Rule	Or
| | |	Stop Inner Iterations	TRUE
| | |	Stop Outer Iterations	FALSE
| | |	Criterion Satisfied	FALSE
| | `-1 Minimum Limit	Minimum Value	1.00E-14
| +-2 **Force Criterion**	Enabled	TRUE
| | |	Criterion Option	Minimum
| | |	Logical Rule	Or
| | |	Stop Inner Iterations	TRUE

| | |	Stop Outer Iterations	FALSE
| | |	Criterion Satisfied	FALSE
| | `-1 Minimum Limit	Minimum Value	1.00E-14
| +-3 **Maximum Steps**	Enabled	FALSE
| |	Maximum Steps	1000
| |	Logical Rule	Or
| |	Criterion Satisfied	FALSE
| `-4 **Stop File**	Enabled	TRUE
|	Stop Inner Iterations	TRUE
|	Path	ABORT
|	Logical Rule	Or
|	Criterion Satisfied	FALSE
+-14 Solution Histories		
+-15 Solution Views		
| `-1 **Current Solution**	Iteration	320
|	Time Step	0
|	Solution Time	0
+-16 Reports	Reports	6
| +-1 **Drag**	Units	N
| |	Coordinate System	Laboratory
| |	Direction	[1.0, 0.0, 0.0]
| |	Force Option	Pressure + Shear
| |	Reference Pressure	0.0 Pa
| |	Number of Bands	0
| |	Parts	[Fluid: Foil, Fluid: Solid/Fluid [1]]
| |	Representation	Volume Mesh
| |	Smooth Values	FALSE
| +-2 **Lift**	Units	N
| |	Coordinate System	Laboratory
| |	Direction	[0.0, 0.0, 1.0]
| |	Force Option	Pressure + Shear
| |	Reference Pressure	0.0 Pa
| |	Number of Bands	0

| |	Parts	[Fluid: Foil, Fluid: Solid/Fluid [1]]
| |	Representation	Volume Mesh
| |	Smooth Values	FALSE
| +-3 **Maximum 1**	Units	
| |	Scalar Field Function	<Select Function>
| |	Parts	[]
| |	Representation	Volume Mesh
| |	Smooth Values	FALSE
| +-4 **Side Force**	Units	N
| |	Coordinate System	Laboratory
| |	Direction	[0.0, 1.0, 0.0]
| |	Force Option	Pressure + Shear
| |	Reference Pressure	0.0 Pa
| |	Number of Bands	0
| |	Parts	[Fluid: Foil, Fluid: Solid/Fluid [1]]
| |	Representation	Volume Mesh
| |	Smooth Values	FALSE
| +-5 **Solver Iteration CPU Time**	Units	s
| `-6 **Total Solver CPU Time**	Units	s
+-17 Monitors	Monitors	18
| |	Monitors To Print	[Continuity, X-momentum, Y-momentum, Z-momentum, Tke, Tdr, Water, Energy, Force, Displacement, FSI Displacement, Lift Monitor, Drag Monitor, Side Force Monitor, Total Solver CPU Time Monitor]
| |	Output Direction	Horizontal
| |	Heading Print Frequency	10
| +-1 **CPU/Iter**	Parts	[]
| | |	Enabled	TRUE
| | |	Sample Count	0
| | |	Trigger	Iteration

				Enable Sliding Sample Window	TRUE
				Title	Mean of Report: Solver Iteration CPU Time
				Field Function	Report: Solver Iteration CPU Time
		+-1 Iteration Frequency	Iteration Frequency	1
				Start Iteration	0
				Enable Stop	FALSE
				Stop Iteration	0
		`-2 Sliding Window	Sliding Sample Window Size	5
	+-2 **Drag Monitor**	Report	[Drag]
				Enabled	TRUE
				Trigger	Iteration
				Normalization Option	Off
				Maximum Plot Samples	5000
		`-1 Iteration Frequency	Iteration Frequency	1
			Start Iteration	0
			Enable Stop	FALSE
			Stop Iteration	0
	+-3 **Iteration**	Maximum Plot Samples	5000
	+-4 **Lift Monitor**	Report	[Lift]
				Enabled	TRUE
				Trigger	Iteration
				Normalization Option	Off
				Maximum Plot Samples	5000
		`-1 Iteration Frequency	Iteration Frequency	1
			Start Iteration	0
			Enable Stop	FALSE
			Stop Iteration	0
	+-5 **Physical Time**	Maximum Plot Samples	5000
	+-6 **Side Force Monitor**	Report	[Side Force]
				Enabled	TRUE
				Trigger	Iteration

| | |	Normalization Option	Off
| | |	Maximum Plot Samples	5000
| | `-1 Iteration Frequency	Iteration Frequency	1
| |	Start Iteration	0
| |	Enable Stop	FALSE
| |	Stop Iteration	0
| +-7 **Total Solver CPU Time Monitor**	Report	[Total Solver CPU Time]
| |	Enabled	TRUE
| |	Time Report	Total Solver CPU Time
| |	Trigger	Iteration
| |	Normalization Option	Off
| |	Maximum Plot Samples	5000
+-18 Summaries		
+-19 Representations		
| +-1 **Geometry**		
| | +-1 **CFD Mesh.Remesh**		
| | +-2 **FE Mesh.Remesh**		
| | `-3 **Latest**		
| +-2 **Initial Surface**	Faces	0
| | |	Edges	0
| | `-1 Regions		
| | +-1 Fluid	Faces	0
| | | |	Edges	0
| | | +-1 Boundaries		
| | | `-2 Feature Curves		
| | `-2 Solid	Faces	0
| | |	Edges	0
| | +-1 Boundaries		
| | `-2 Feature Curves		
| `-3 **Volume Mesh**	Cells	6343345
| |	Interior Faces	15955334

| |	Vertices	4463406
| +-1 Finite Volume Regions		
| | +-1 Fluid	Cells	3738263
| | | |	Interior Faces	11197561
| | | |	Vertices	3812251
| | | |	Edges	0
| | | `-1 Finite Volume Boundaries		
| | | +-1 Flow Domain.Inlet	Faces	7869
| | | +-2 Flow Domain.Outlet	Faces	907
| | | +-3 Foil	Faces	0
| | | `-4 Solid/Fluid [1]	Faces	96794
| | `-2 Solid	Cells	2605082
| | |	Interior Faces	4757773
| | |	Vertices	651155
| | |	Edges	0
| | `-1 Finite Volume Boundaries		
| | +-1 Default	Faces	0
| | `-2 Solid/Fluid [0]	Faces	904782
| `-2 Cell Sets		
+-20 Units	Preferred System	Systeme Internationale
+-21 Coordinate Systems		
| `-1 **Laboratory**		
| `-1 Local Coordinate Systems		
| `-1 **Body 1-CSys**	X Axis Direction	[1.0, 0.0, 0.0]
| |	Y Axis Direction	[0.0, 1.0, 0.0]
| |	Z Axis Direction	[0.0, 0.0, 1.0]
| |	Origin	[0.0, 0.0, -6.043986511547748E-5] m,m,m
| |	Reference System	Laboratory
| `-1 Local Coordinate Systems		

+-22 Tables	Tables	0
+-23 Filters		
+-24 Field Functions		
+-25 Volume Shapes		
+-26 Data Set Functions	Data Directory	function_data
+-27 Update Events	Event Count	0
|	Event Names	
+-28 User Code		
+-29 Layouts		
| `-1 default		
+-30 Data Mappers		
+-31 Motions		
| +-1 **Morphing**	Morphing Order	Regionwise
| |	Automatic Thin-out	TRUE
| |	Automatic Thin-out Cl	2
| |	Automatic Thin-out Cp	0.05
| |	Automatic Thin-out Cplane	1
| |	Automatic Thin-out Cb	0.05
| |	Automatic Thin-out MinCV	50
| |	Automatic Thin-out CorSiz	50
| |	Automatic Thin-out TMax	20
| |	Linear Fitter	FALSE
| |	Extension ID	0
| |	Extension Key	
| +-2 **Solid Displacement**		
| `-3 **Stationary**		
+-32 Reference Frames		
| +-1 **Body 1-ReferenceFrame**	Axis Direction	[0.0, 0.0, 0.0]
| |	Axis Origin	[0.0, 0.0, -6.043986511547748E-5] m
| |	Rotation Rate	0.0 radian/s
| |	Translation Velocity	[-0.0, -0.0, -0.024175946046190992] m/s

| |	Coordinate System	Laboratory
| `-2 **Lab Reference Frame**		
+-33 Data Focus		

Solution

Accumulated CPU Time over all processes (s)	264588.826
Elapsed Time (s)	17639.27804
Iterations	320

APPENDIX C: 2D VALIDATION RESULTS

2D VALIDATION RESULTS

The following tables present the percentage change of the lift to drag ratio from two-dimensional theory to the CFD analysis. The resultant force vector from the lift and sideforce found using Star CCM+ is taken as the total lift. The expanded area, or the surface area of one side of the foil was used to non-dimensionalize the resultant total lift. In all cases, the ideal two-dimensional foil outperformed the more realistic three-dimensional CFD model.

Undeformed Cases

Speed (kt)	α (deg)	Speed (m/s)	Lift (kN)	Sideforce (kN)	Resultant (kN)	Cl	Drag	Cd	Cl/CD	% Change
15	-1	7.72	6.71	4.13	7.88	0.19	0.49	0.01	16.07	31%
	0	7.72	7.29	5.51	9.14	0.23	0.55	0.01	16.62	29%
	1	7.72	7.94	6.95	10.55	0.26	0.60	0.01	17.46	27%
	2	7.72	8.69	8.52	12.17	0.30	0.69	0.02	17.70	25%
	3	7.72	9.27	9.85	13.53	0.33	0.77	0.02	17.47	23%
30	-1	15.44	25.60	16.48	30.45	0.19	1.83	0.01	16.60	19%
	0	15.44	28.33	22.33	36.08	0.22	2.00	0.01	18.02	20%
	1	15.44	30.87	27.93	41.63	0.26	2.23	0.01	18.65	19%
	2	15.44	33.92	34.39	48.30	0.30	2.55	0.02	18.91	19%
	3	15.44	36.39	39.78	53.91	0.33	2.90	0.02	18.62	18%
45	-1	23.15	42.82	27.72	51.01	0.14	3.01	0.01	16.94	16%
	0	23.15	47.43	37.61	60.54	0.17	3.29	0.01	18.42	17%
	1	23.15	51.80	47.12	70.03	0.19	3.65	0.01	19.17	17%
	2	23.15	56.85	57.87	81.12	0.22	4.22	0.01	19.23	18%
	3	23.15	60.95	66.86	90.47	0.25	4.78	0.01	18.92	18%

APPENDIX D: STAR CCM+ VALIDATION RESULTS

STAR CCM+ VALIDATION RESULTS

The following tables show the lift, drag, and side force results from Star CCM+ CFD analysis using both the files provided by Nate Fast and the files generated by us, in addition to the results presented in Fast's Thesis. The first five test were conducted in accordance with the files attained from Fast's Thesis, the final test consists of a loading condition from our test matrix evaluated in both CFD environments.

Summary of Star CCM+ Results

Lift (kN)

Tip Angle	Yaw Angle	Fast Thesis (kN)	Fast Star CCM+ (kN)	BS Star CCM+ (kN)	%Difference Fast Thesis	%Difference Fast Star CCM+
40°	0°	170	202.6	171.8	1%	18%
				204.1	17%	1%
	6°	228	228.6	198.4	15%	15%
				230.9	1%	1%
	10°	N/A	233.7	208.7	N/A	12%
				239.4	N/A	2%
20°	0°	193.9	193.6	162.3	19%	19%
				196.3	1%	1%
0°	4°	265.6	265.6	236	13%	13%
				270.4	2%	2%
40° (BS Run)	18°	N/A	118.1	76.5	N/A	54%

Drag (kN)

Tip Angle	Yaw Angle	Fast Thesis (kN)	Fast Star CCM+ (kN)	BS Star CCM+ (kN)	%Difference Fast Thesis	%Difference Fast Star CCM+
40°	0°	12.3	13.9	11.6	6%	20%
				12.6	2%	10%
	6°	28.5	28.1	26.3	8%	7%
				27.9	2%	7%
	10°	N/A	49.9	49.3	N/A	1%
				49.4	N/A	1%
20°	0°	12.9	12.6	11	17%	15%

				12	8%	5%
0°	4°	21.3	21.1	18.4	16%	15%
				19.9	7%	6%
40° (BS Run)	18°	N/A	190.4	157.8	N/A	21%

Side Force (kN)

Tip Angle	Yaw Angle	Fast Thesis (kN)	Fast Star CCM+ (kN)	BS Star CCM+ (kN)	% Difference Fast Thesis	Fast Star CCM+
40°	0°	103	109.4	104.4	1%	5%
				109.6	6%	0%
	6°	394	394.4	391.7	1%	1%
				396.7	1%	1%
	10°	N/A	555.4	564.8	N/A	2%
				567.3	N/A	2%
20°	0°	153.3	153.2	140.8	6%	6%
				154	0%	1%
0°	4°	360	360.7	342.3	5%	5%
				363.6	1%	1%
40° (BS Run)	18°	N/A	623.1	502.5	N/A	24%

APPENDIX E: STAR CCM+ RESULTS

STAR CCM+ RESULTS

Testing Matrix		*Undeformed*			*Deformed*			*% Change*		
Speed (kt)	α (deg)	Lift (kN)	Drag (kN)	Sideforce(kN)	Lift (kN)	Drag (kN)	Sideforce(kN)	Lift	Drag	Sideforce
15	-1	6.71	0.49	4.13	6.79	0.51	3.87	1%	4%	-7%
	0	7.29	0.55	5.51	7.47	0.55	5.27	2%	1%	-4%
	1	7.94	0.60	6.95	8.16	0.61	6.69	3%	1%	-4%
	2	8.69	0.69	8.52	8.78	0.69	8.31	1%	0%	-3%
	3	9.27	0.77	9.85	9.54	0.78	9.56	3%	0%	-3%
30	-1	25.60	1.83	16.48	30.53	1.98	13.41	16%	7%	-23%
	0	28.33	2.00	22.33	33.72	2.16	18.65	16%	7%	-20%
	1	30.87	2.23	27.93	38.21	2.52	26.13	19%	11%	-7%
	2	33.92	2.55	34.39	44.54	3.20	35.19	24%	20%	2%
	3	36.39	2.90	39.78	44.59	3.20	35.25	18%	9%	-13%
45	-1	42.82	3.01	27.72	58.43	3.54	20.41	27%	15%	-36%
	0	47.43	3.29	37.61	62.69	3.77	27.35	24%	13%	-38%
	1	51.80	3.65	47.12	73.26	4.63	42.85	29%	21%	-10%
	2	56.85	4.22	57.87	69.52	4.70	48.53	18%	10%	-19%
	3	60.95	4.78	66.86	70.75	4.97	55.85	14%	4%	-20%

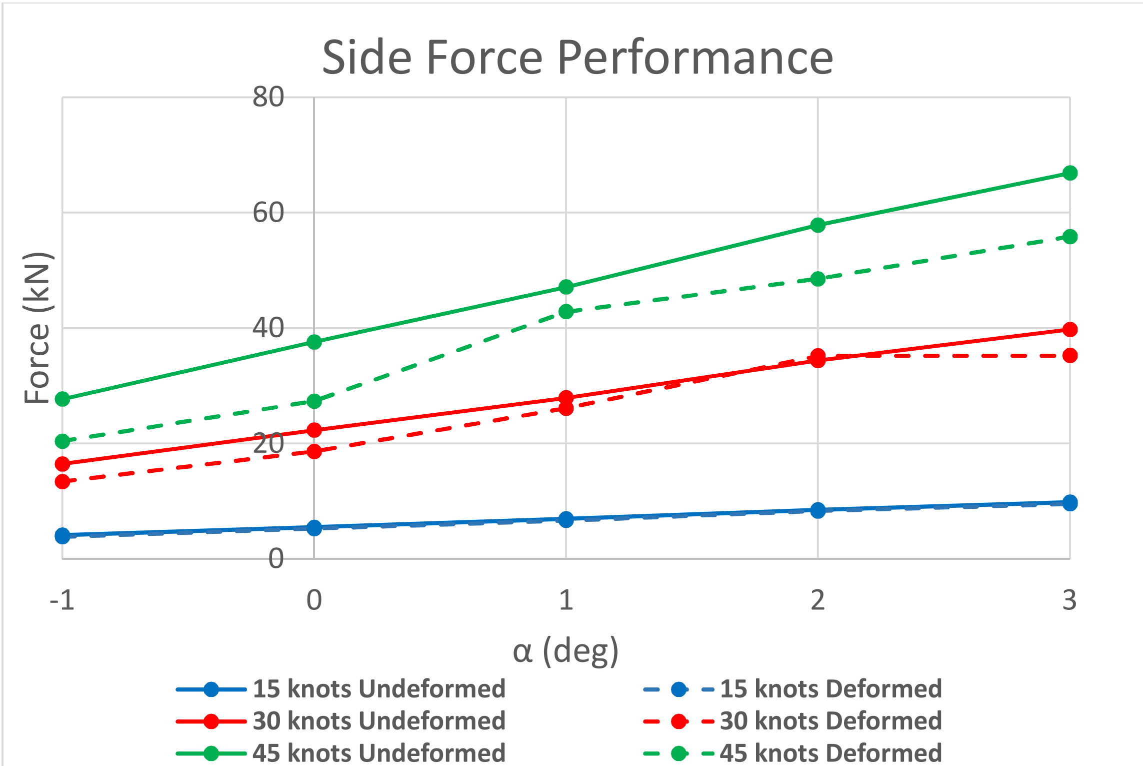
Side Force Performance
Force (kN)
80
60
40
20
0
-1
0
1
2
3
α (deg)
15 knots Undeformed
30 knots Undeformed
45 knots Undeformed
15 knots Deformed
30 knots Deformed
45 knots Deformed

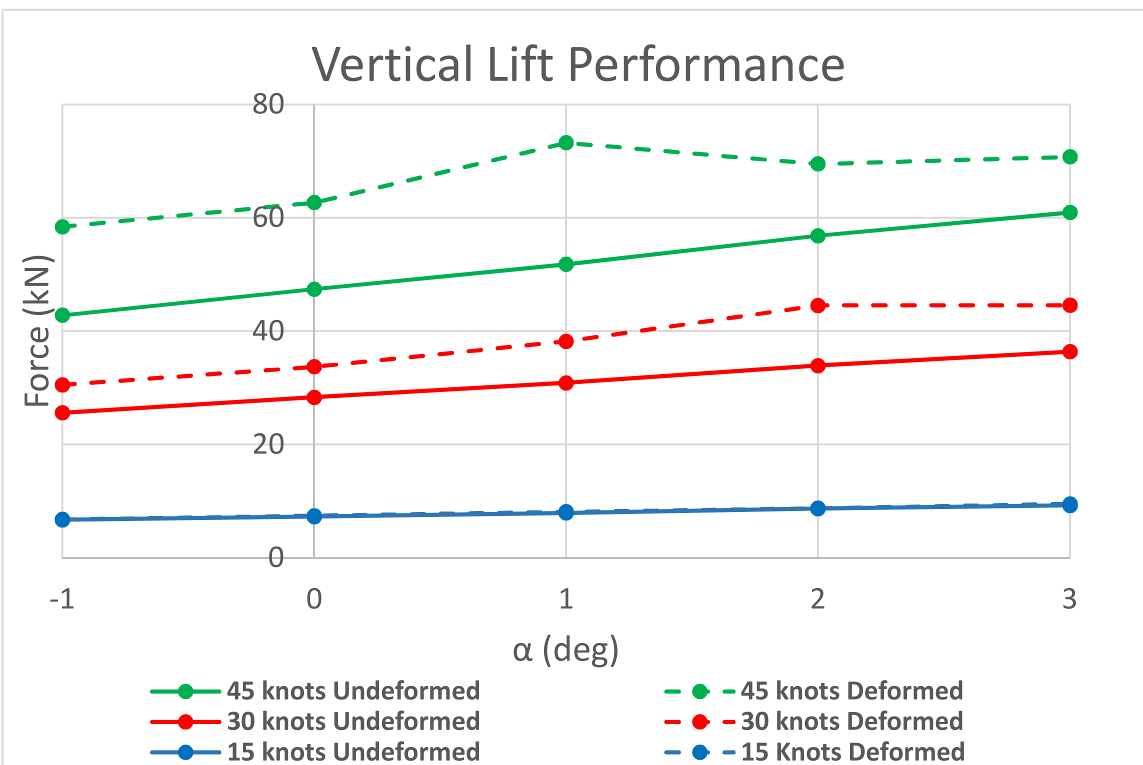
Vertical Lift Performance
Force (kN)
80
60
40
20
0
-1
0
1
2
3
α (deg)
45 knots Undeformed
30 knots Undeformed
15 knots Undeformed
45 knots Deformed
30 knots Deformed
15 Knots Deformed

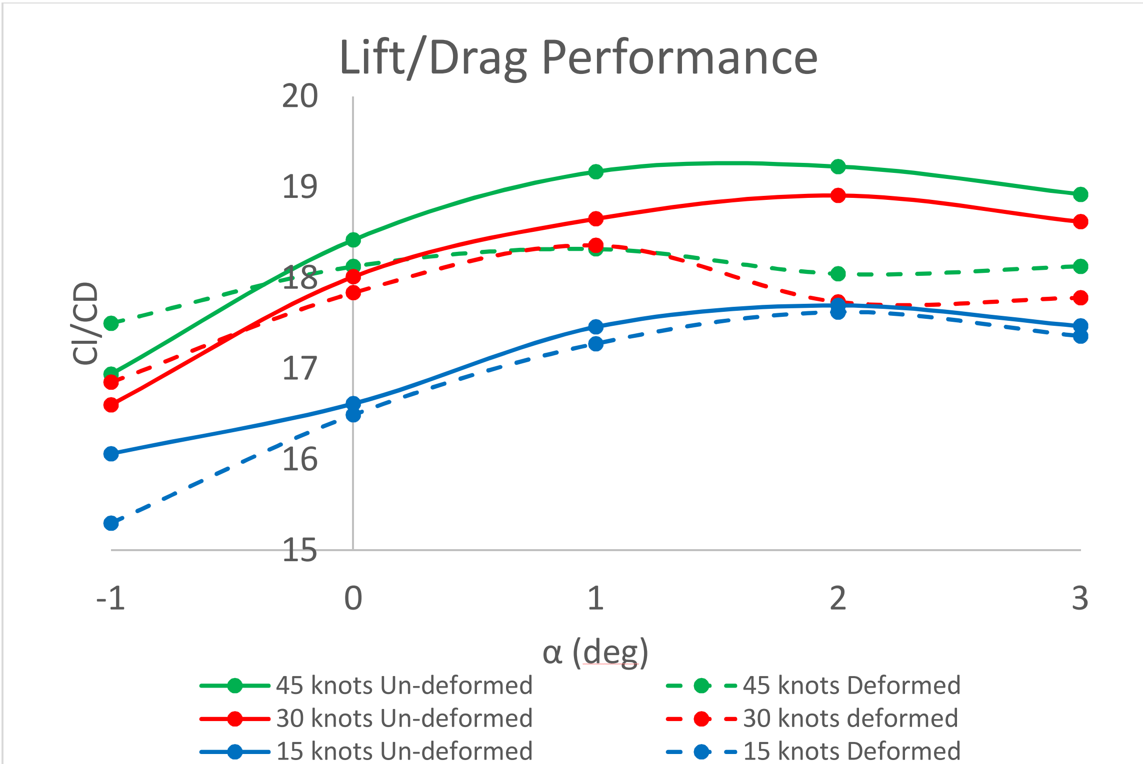
Lift/Drag Performance
Cl/CD
20
19
18
17
16
15
-1
0
1
2
3
α (deg)
45 knots Un-deformed
45 knots Deformed
30 knots Un-deformed
30 knots deformed
15 knots Un-deformed
15 knots Deformed